

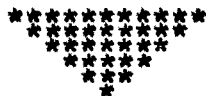
PART-1



CHAPTER - 5

GROWTH OF  $\alpha$ -AHT SINGLE CRYSTALS  
IN SILICA GEL

	<u>PAGE</u>
5.1 Introduction ... ..	90
5.2 Experimental ... ..	91
5.2.1 Preparation of silica gel ...	91
5.3 Results and discussion ... ..	93
5.3.1 Crystal growth ... ..	93
5.3.2 Crystal morphology and habits .	96
5.3.3 Effect of gel pH on growth ...	101
(a) pH of a solution ... ..	101
(b) Gel pH and crystal growth.	106
5.4 Conclusions ... ..	108
References	



## 5.1 INTRODUCTION

The gel method has proved to be a promising technique for growing single crystals which are insoluble or sparingly soluble in water and which cannot be grown from melt or from the vapour.<sup>1</sup> (Suri et al., 1970). It has been reported<sup>2-6</sup> (Henisch, 1970 ; Kratochvil and Sprusil, 1968 ; Liow and Faust, 1971 ; Halferstadt and Henisch, 1968 ; Pillai and Itlyachen, 1978) that a variety of crystals suitable for research and technology can be grown in silica gel. Gels can act as excellent supporting media through which the reacting materials can diffuse at a suitable rate promoting crystal growth. Crystals grown by gel technique are normally geometrically well-defined and exhibit many crystallographic features. Research in this field has progressed by leaps and bounds with the pioneering work of Henisch (1970).<sup>2</sup>

The growth of single crystals of ammonium-hydrogen-d-tartrate is of considerable interest in view of the fact that it exhibits piezoelectric properties and its growth morphology and other properties are relatively unknown. The importance

of gel technique and its preference to other crystal growth techniques have been emphasized in Chapter-4. In this chapter the performance and potentiality of the gel technique is tested in producing larger and more perfect single crystals of ammonium-hydrogen-d-tartrate (ammonium acid tartrate).

## 5.2 EXPERIMENTAL

### 5.2.1 Preparation of Silica Gel

The solution of commercial water glass in distilled water was filtered with ordinary filter paper to separate the floating and suspended impurities. As a result transparent golden coloured solution of sodium meta-silicate was obtained and could be preserved as a stock solution for quite a long time. To this solution of sodium meta-silicate, was added a required quantity of distilled water so as to obtain a solution of specific gravity  $1.4 \text{ gm cm}^{-3}$ . When this solution is mixed with any mineral or organic acid, gel formation takes place due to polymerization as ~~formation takes place due to polymerization as~~ described earlier (cf Chapter-4). Time required for gelation depends on a number of factors such as

density and pH of gel solution, acid used for gelation, ambient temperature etc. Gels of low density and low pH values required relatively longer time for setting.

In the present work, solution of d-tartaric acid ( $C_4H_6O_6$ ) (GR quality 99.5% pure) was prepared by dissolving it in an appropriate amount of distilled water to give required molar concentration (cf Chapter-2) as shown in the table 5.1

Table 5.1

Molar concentration of TA (d-tartaric acid) in distilled water at 35°C

Sr. No.	Amount of d-tartaric acid in gm	Volume of solution in c.c.	Molar Concentration (M)
1	225.135	1000	1.5
2	300.180	1000	2.0
3	375.225	1000	2.5
4	450.270	1000	3.0
5	525.315	1000	3.5

Gels were prepared by mixing sodium meta-silicate solution (sp. gra. 1.04) with d-tartaric acid solution in different proportions. The pH of the mixture was measured by pH meter. In what follows, tartaric acid always means d-tartaric acid.

### 5.3 RESULTS AND DISCUSSION

#### 5.3.1 Crystal Growth

Crystallization was carried out in standard test tubes of different dimensions (2.5 cm diameter and length 22.5 cm ; 3.6 cm diameter and length 20 cm). Silica gels were prepared by mixing sodium metasilicate solution (sp. gr. 1.04) with tartaric acid (TA) solution having different molar concentrations in different amounts as described in the last section. The gel is usually set within 4 to 18 days, depending on the gel density, pH of the gel solution and the environmental temperature. After ensuring proper gel setting, the growth experiment was started by adding the feed solution (FS) ammonium chloride (GR quality,) having different concentrations varying from 1.5M to 3.5M (Table 5.2) above the set gel with the help of a pipette (Least count 0.1 ml).

Table 5.2

Molar concentration of FS (feed solution - ammonium chloride) in distilled water at 35°C

Sr. No.	Amount of ammonium chloride in gm	Volume of solution in c.c.	Molar Concentration (M)
1	80.240	1000	1.5
2	106.990	1000	2.0
3	133.740	1000	2.5
4	160.490	1000	3.0
5	187.240	1000	3.5

The drops from the pipette were allowed to fall gently along the sides of the test tube in order to prevent breaking of the surface and inner structure of the gel. Slowly the FS will diffuse in gel and react with gel incorporated TA, forming transparent geometrically well defined single crystals of ammonium hydrogen-d-tartrate (d-AHT) in the test tube (fig. 5.1) The chemical reaction between these reagents is as follows :

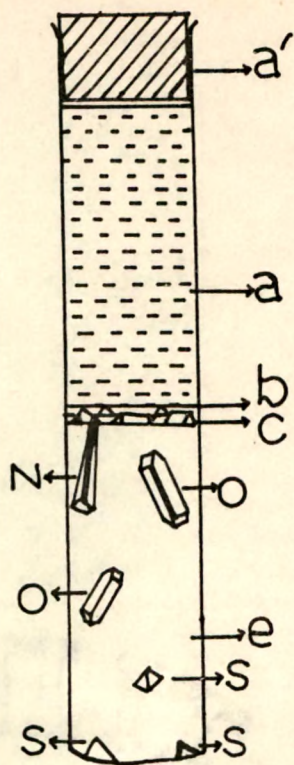


Fig. 5.1 Schematic drawing of test tube containing

- (a') Rubber cork
- (a) Ammonium-chloride-Feed solution (FS)
- (b) Liquid expelled from gel due to syneresis
- (c) Crystals on gel-liquid interface
- (d) Crystals in gel : needle-shaped (N) ; orthorhombic disphenoidal (o) and sphenoidal (s)
- (e) d-tartaric acid impregnated sodium metasilicate gel.

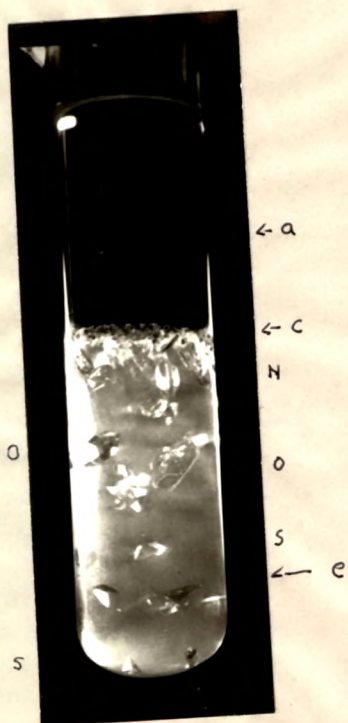
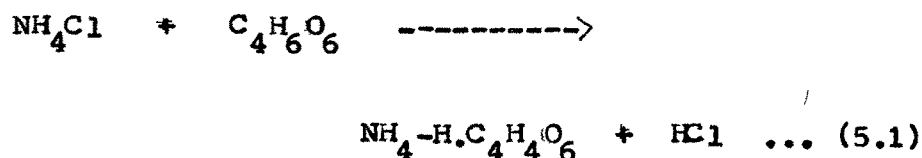


Fig. 5.2 Photograph of a test tube showing

- (a) Ammonium-chloride-feed solution (FS)
- (c) Crystals on gel-liquid interface
- (d) Crystals in gel : needle-shaped (N), orthorhombic disphenoidal (o) and sphenoidal (s)
- (e) d-tartaric acid impregnated sodium metasilicate gel.



There are basically three regions in a test tube where the crystal nuclei have the opportunities to grow. They are as follows :

- (a) The interface between the gel and the FS is one of the places where reaction between FS and gel takes place, resulting in the production of crystal nuclei. The interface is also the place where the phenomenon of syneresis takes place. This phenomenon constitutes one of the important properties of a gel. It is a spontaneous liberation of liquid from the gel. Obviously this liquid is tartaric acid. It can also be considered as internal dehydration. It is associated with the shrinking of the gel, thereby affecting the pore size. In fig. 5.2 the interface is represented by 'a'.
- (b) The second region is obviously the central part of the test tube. The FS percolates through pores of the gel and reacts with gel acid. The crystal nuclei begin to develop in the gel pores

of the central part of the tube (Fig. 5.2).

- (c) The FS can also slip through some space between gel and tube walls. The solution reacts with the impregnated acid in the gel, with formation of crystal nuclei near the walls and bottom of the test tube (Fig. 5.2).

From these three regions crystals were collected after allowing sufficient time (about 6 to 8 weeks) to develop the nuclei and subsequent growth. The graphical study of the effect of different growth parameters on nucleation is given in the next chapter. Qualitative features regarding morphology etc. are discussed here.

### 5.3.2 Crystal Morphology and Habits

A large range of concentration of reactants (tartaric acid impregnated gel and ammonium chloride) is used to determine optimum conditions of growth of good quality single crystals of d-AHT. In what follows the sodium metasilicate solution (SMS) in water has a specific gravity 1.04 ~~g/cm<sup>3</sup>~~. The concentration of tartaric acid solution (TA) in SMS was varied. The gel concentration refers to the concentration of TA

in it. Further with a fixed concentration of TA, the quantity of TA added to SMS was also varied. This amount is indicated in percentage of the entire solution (SMS & TA). The experimental work was carried out at room temperature RT - 35°C .

It is observed that minimum concentration of tartaric acid for initiating the growth is 0.5M. Below this concentration, growth is almost impossible. It is possible to grow crystals by varying concentrations from 0.5M to 5.099 M which corresponds to the saturated solution of TA in water at R.T. For lower gel concentration (between 0.5M to 1.5M) the quantity of TA should be more than 50% to obtain crystals of good geometrical shape. The concentration of FS in the above case was varied from 1.5M to 3.5M. For concentrations less than 1.5M, the ability of the FS to diffuse is greatly diminished, thereby decreasing the probability of formation of crystal nuclei and subsequent growth. For concentration > 3.5M, the diffusion is heavy, resulting in the growth of translucent crystals. In between the above extreme cases good quality transparent crystals with well-defined geometrical shapes could be obtained. For temperatures lower than

RT (35°C) the concentration values of TA would obviously change to lower values and for FS inverse is the case. The detailed observations are described below :

There are basically three habits of the d-AHT crystals grown in silica gel. They are as under :

- (i) Needle-shaped crystals (Fig. 5.3a)
- (ii) Orthorhombic disphenoidal crystals (Fig. 5.3b)
- (iii) Sphenoidal (Tetrahedral) crystals (Fig. 5.3c)

It should be noted that only three habits mentioned above are observed for all possible combinations of different factors affecting the growth of these crystals in gel.

The needle-shaped crystals start growing from a bunch of nuclei at the interface between gel and FS. With the timely arrival of the FS, they start getting separated as fine needles. The gradual deposition of crystal material thickens the needle and also extends its growth along one direction viz. C-direction, which is the growth direction of d-AHT crystals of different habits. Further the direction

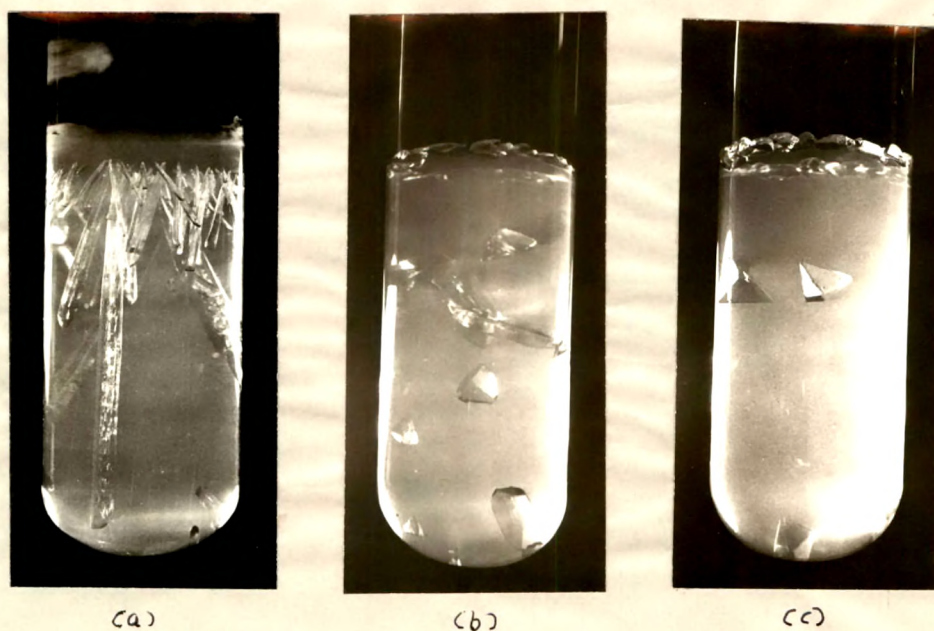


Fig. 5.3 Photographs of d-AHT crystals of different habits obtained by allowing TA of 3M concentration in a silica gel of sp. gravity 1.04 to react with 2.5M FS

- (a) 20% TA of gel pH 3.0 to obtain needle-shaped crystals.
- (b) 40% TA of gel pH 2.2 to obtain orthorhombic disphenoidal.
- (c) 60% TA of gel pH 1.7 to obtain sphenoidal crystals.

is inclined with the vertical, i.e. with the test tube. Many observations regarding orientation of these crystals with vertical axis of test tube are made. There does not appear to be any preferred orientation. Fig. 5.4a,b represent the different stages of growth of needle-shaped crystals.

The orthorhombic disphenoidal and sphenoidal crystals are normally found at the central part of gel and bottom part of the test tube. Some interesting growth features for these two habits are noticeable. (a) The orthorhombic disphenoidal crystals grow by having (i) growth in bunches (Fig. 5.5a,b) and also (ii) penetration of a crystal into another at a definite angle (Fig. 5.6) (b) Rows of sphenoidal crystals (Fig. 5.7a,b). There is one common feature in these habits. During growth the twinning between the growing crystals sometimes takes place resulting in the continuous twinned growth.

From Fig. 5.8 it appears the excessive growth of crystal in the horizontal direction has damaged the gel net work and hence formation similar to that of cusp resulted. There is also a possibility of formation of two crystals in the horizontal

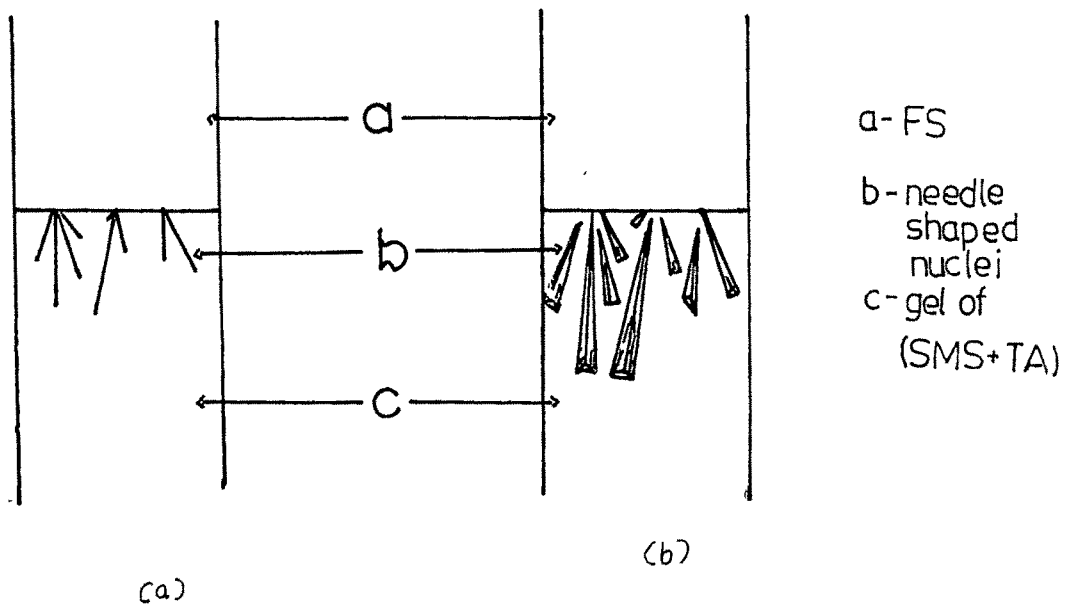


Fig. 5.4(1,b) Schematic drawing of the  
 (a) bunching of nuclei  
 (shown by lines)  
 (b) subsequent separation  
 into fine needles.

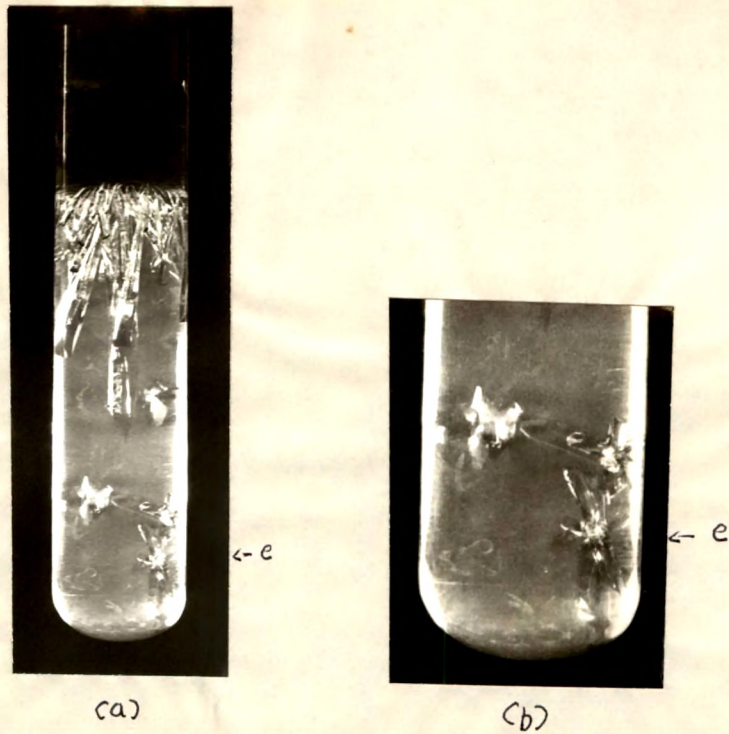


Fig. 5.5(a) Photograph of bunch-growth of orthorhombic disphenoidal crystals  
 (b) Enlarged portion of bunch-growth (e), shown in (a)

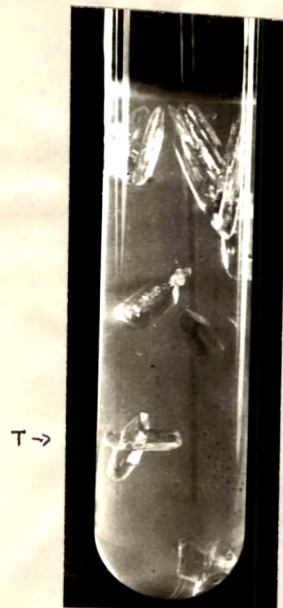


Fig. 5.6 Photograph showing penetration of a growing orthorhombic disphenoidal crystals, in a twinned form (T)

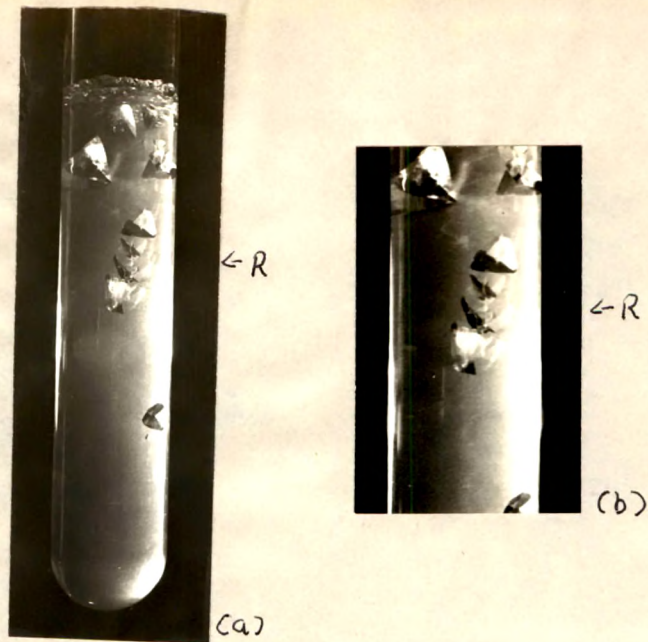


Fig. 5.7(a) Photograph showing growth of twinned sphenoidal crystals in rows (R)

(b) Enlarged portion of sphenoidal crystals in rows (R) shown in (a)

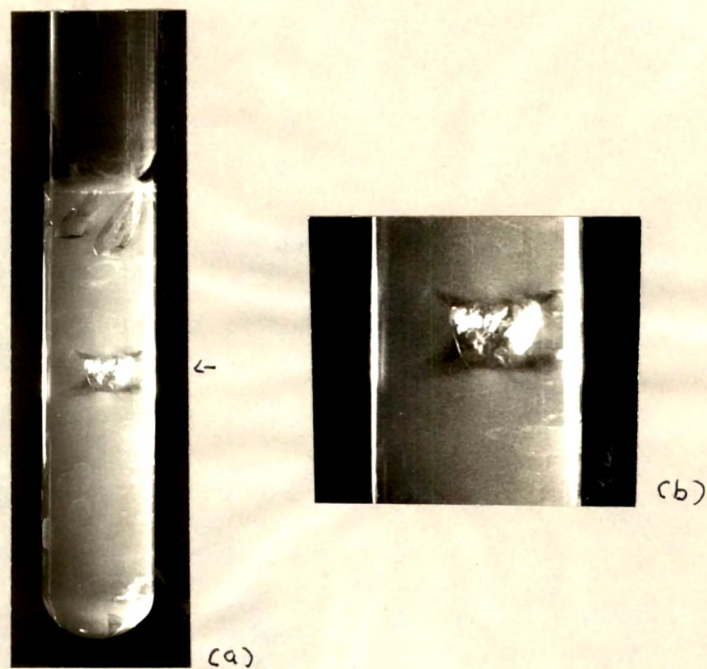


Fig. 5.8(a) Photograph of cusp formation around twinned sphenoidal crystals

(b) Enlarged portion of cusp around twinned sphenoidal crystals.

direction (Fig. 5.8a,b), a small one and large sized one in twinned position. In the absence of full knowledge of twinning laws operating for these crystals, it is difficult to arrive at a definite conclusion.

The size of a face of a grown crystal depends upon the amount of feed material available to a growing crystal. This can be qualitatively connected with various parts of the test tube at which crystals of different habits have grown. Thus when fairly large amount of FS is available, needle-shaped crystal grow. With decreasing amount the crystal habit becomes orthorhombic disphenoidal. With a further drop in the availability of feed solution only sphenoidal crystals could be obtained. This also suggests rather an elegant method to grow crystals of desired habit. In majority of the grown crystals C-axis happens to be the growth axis, which is slightly inclined with the vertical. However, there are a few exceptions to this general observation. The reason for this, could not be deduced from the available data. Further, the habit and quality of grown crystals depend not only on the amount of material (FS) available at a place but also

on the rate at which the material is made available at that place. It is observed that the crystals with very high growth rate are of inferior quality. The converse of this statement is also true.

### 5.3.3 Effect of gel pH on Growth

#### (a) pH of a solution

There are several factors which influence size and morphology of growing crystals in a gel medium. They are gel pH, concentration and quantity of FS and d-TA, specific gravity of SMS, number of nuclei, temperature. Out of these factors, it is found that the gel pH is influencing quite significantly the size and morphology of d-AHT crystals. In order to understand and appreciate the importance of gel pH, it is desirable to have a clear meaning of pH. The term pH, also known as hydrogen ion concentration, is always mentioned with respect to the universal solvent water which is amphoteric and poor conductor of electricity. Dissociation of water creates the formation of  $H^+$  and  $OH^-$  ions. Pure water is capable of acting either as a weak acid or a weak base by virtue of its ionization to a slight extent into  $H^+$  and  $OH^-$  ions :-



The above equation is applicable to any aqueous solution. Application of the law of mass action to the above reversible reaction yields

$$\frac{C_{H^+} \times C_{OH^-}}{C_{H_2O}} = K_w \quad \dots (5.3)$$

where symbol  $C$  represents concentration and  $K_w$  the ionic product of water or dissociation constant of water. Electrical measurements give  $K_w = 10^{-14}$  (gm - ion per litre) at room temperature. The concentration of undissociated or unionized water is practically constant and is very close to unity ( $C_{H_2O} = 1$ ). Substitution of values of  $K_w$  and  $C_{H_2O}$  gives

$$C_{H^+} \times C_{OH^-} = 10^{-14} \quad \dots (5.4)$$

Thus the product of the concentrations of  $H^+$  and  $OH^-$  ions in water or in any aqueous solution is constant at constant temperature. Further (5.4) indicates that in a completely neutral solution, the hydrogen and hydroxyl ion concentrations are equal and each has a value  $10^{-7}$  gm-ion per litre :

$$C_{H^+} = C_{OH^-} = \sqrt{K_w} = 10^{-7} \text{ gm-ion per litre} \quad \dots (5.5)$$

If hydrogen ion concentration  $C_{H^+}$  exceeds this value, the solution is said to be acidic and obviously in such a solution hydroxyl ion concentration  $C_{OH^-}$  will be less than  $10^{-7}$  gm-ion per litre. On the other hand if  $C_{H^+}$  is less than  $10^{-7}$ ,  $C_{OH^-}$  will be greater than  $10^{-7}$  and the aqueous solution is said to be alkaline. Thus the product  $C_{H^+} \cdot C_{OH^-}$  for a solution must be  $10^{-14}$  at room temperature whether the solution is acidic, alkaline or neutral.

Hydrogen ion concentration, expressed in terms of normality or gramme equivalents per litre, can vary from about 1 gm-ion per litre in a normal solution of strong acid to  $10^{-14}$  in a normal solution of alkali. It is evident that expressing hydrogen ion concentration in the form  $1 \times 10^{-n}$  normal is inconvenient. Hence it was suggested by Sorenson that hydrogen ion concentration should be expressed in terms of hydrogen ion exponent. This is a number obtained by giving a positive value to the negative power of 10 in the expression  $10^{-n}$  normal and is usually written as pH. Hence the pH value is defined as the logarithm to the base 10 of the hydrogen ion concentration with a negative sign or the logarithm

to the base 10 of the reciprocal of the hydrogen ion concentration expressed in gramme-ions per litres expressed algebraically

$$\text{pH} = -\log_{10} [\text{H}^+] = \log_{10} \left[ \frac{1}{[\text{H}^+]} \right]$$

$$\text{or } [\text{H}^+] = 10^{-\text{pH}} \quad \dots (5.6)$$

where  $\text{H}^+$  is the hydrogen ion concentration in gramme-ions per litre. In this way the hydroxyl ion concentration,  $\text{pOH}$  can also be expressed

$$\text{pOH} = -\log_{10} [\text{OH}^-] \quad \dots (5.7)$$

or

$$[\text{OH}^-] = 10^{-\text{pOH}} \quad \dots (5.8)$$

Thus equation (5.5) can be written as

$$\text{pH} + \text{pOH} = \text{pK}_w = 14$$

An idea of the acidity or alkalinity of a solution can be obtained at a glance from the following table :

	Hydrochloric acid solution							Pure water		
	$\frac{N}{1}$	$\frac{N}{10}$	$\frac{N}{10^2}$	$\frac{N}{10^3}$	$\frac{N}{10^4}$	$\frac{N}{10^5}$	$\frac{N}{10^6}$			
pH	0	1	2	3	4	5	6	7		
	Pure Water			Caustic soda solution						
				$\frac{N}{10^6}$	$\frac{N}{10^5}$	$\frac{N}{10^4}$	$\frac{N}{10^3}$	$\frac{N}{10^2}$	$\frac{N}{10}$	$\frac{N}{1}$
pH		7		8	9	10	11	12	13	14

From the above table it will be observed that high pH values correspond to low hydrogen ion concentration and an alteration of one unit in the pH value amounts to tenfold alteration in hydrogen ion concentration. By this method of expressing the hydrogen ion concentration all degrees of acidity or alkalinity from that of a solution containing 1 gm - equivalent of hydrogen ion per litre to that of a solution containing 1 gm equivalent of hydroxide ion per litre can be expressed by a series of positive number from 0 to 14.

In the present case the gel pH of a mixture containing d-TA and SMS solution (sp. gra. 1.04

was measured by a pH meter (Systronics pH meter with glass-calomel electrodes, model No. 325, L.C. = 0.1 pH), before the commencement of gelation. The values of gel pH mentioned in tables 5.3 and 5.4 were obtained by using the above pH meter.

(b) Gel pH and Crystal Growth

The effect of gel pH on the morphology of grown crystals is qualitatively studied by keeping all other factors constant. In what follows the gel solution means the solution containing tartaric acid of certain concentration mixed with SMS of specific gravity 1.04. In this solution the concentration of SMS remains constant. The pH of the gel solution can be changed by changing the quantity of TA or SMS, or concentration of one of the components or both of the solutions. Further the pH was determined at the time of mixing TA & SMS. The network of silicic acid is formed, giving rise to the formation of gel with a definite extension of network in the available space and a fixed size of pores of network. In the present case the gel pH was varied from 1.56 to 3.72, with varying concentrations and quantities of TA and also varying quantity of SMS. The sizes of the test

tubes in which the gel was set were also fixed. Further for avoiding the temperature fluctuations, test tubes containing gel solution & FS were kept in oven and incubator, the temperatures of which were thermostatically controlled. Under these conditions, the present study was carried out. The observations were extended over a period of two months and the results were reported in tables 5.3 & 5.4. The formation of gel depends not only on the concentration of TA, but also on its quantity. The setting time is found to vary from a few days say 4 days to about 18 days. It is observed that with 1.5M and 60% TA, the number of days required for the formation of gel is about 18 days. When test tube was kept for more days, a fungus growth was found on the surface. Hence the formation period can not be increased beyond 18 days. Further this has also restrained the utilization of gel with  $1.7 \leq \text{pH} \leq 3$  with concentration  $0.1.5\text{M} < \text{TA} < 3.5\text{M}$ , and quantity of TA between 20% & 60%. The study was divided into two parts as mentioned in tables 5.3 & 5.4. Table 5.3 summarizes the results of experiments carried out over a period of more than two months. In this study with a fixed quantity and concentration of TA with formation

Table 5.3

Data on crystal morphology, gel pH molar concentration of TA for a fixed molar concentration of FS<sup>^</sup>

R.T. = 35°C

FS concn = 2 M

TA <sup>*</sup> concn  (in M)	% acid with SMS <sup>*</sup>	Gel pH	Crystal Morphology Maximum linear growth parallel to			Gel setting time  (in days)
			C-axis Needle shaped  (in mm)	[001] Ortho- rhombic disphe- noidal (in mm)	[001] Sphenoidal  (in mm)	
1.5 M	20%	3.72	40	13	7	4
	30%	3.20	--	16	10	6
	40%	2.82	--	31	7	10
	50%	2.51	--	16	10	15
	60%	2.30	--	--	8	18
2.0 M	20%	3.30	36	12	--	5
	30%	2.87	--	16	8	8
	40%	2.56	--	--	14	9
	50%	2.30	--	--	13	14
	60%	2.10	--	--	11	16
2.5 M	20%	3.18	31	13	--	6
	30%	2.70	--	16	8	8
	40%	2.37	--	17	9	10
	50%	2.09	--	--	9	11
	60%	1.85	--	--	10	12
3.0 M	20%	3.00	56	14	--	5
	30%	2.50	--	22	6	6
	40%	2.20	--	17	8	7
	50%	1.90	--	--	10	8
	60%	1.70	--	--	11	9
3.5 M	20%	2.65	--	22	7	6
	30%	2.25	--	10	11	7
	40%	1.95	--	14	12	8
	50%	1.73	--	14	9	9
	60%	1.56	--	--	12	10

\* TA - Tartaric acid solution

\* SMS - Sodium metasilicate solution

^ FS - Feed solution

Table 5.4

Data on crystal morphology, gel pH, molar concentration of FS for a fixed molar concentration of TA

R.T. = 35°C  
TA concn = 3.0 M

% acid with SMS*	Concn of FS† (in M)	gel pH	Crystal Morphology Maximum linear growth parallel to		
			C-axis Needle shaped (in mm)	[001] orthorhombic disphenoidal (in mm)	[101] Sphenoidal (in mm)
20%	1.5	3.0	27	21	--
	2.0		56	14	--
	2.5		63	11	--
	3.0		60	17	--
	3.5		60	17	--
30%	1.5	2.5	--	20	8
	2.0		--	22	6
	2.5		33	42	7
	3.0		37	10	4
	3.5		37	7	--
40%	1.5	2.2	--	9	10
	2.0		--	17	8
	2.5		--	20	8
	3.0		--	14	12
	2.5		--	17	8
50%	1.5	1.9	--	--	12
	2.0		--	--	10
	2.5		--	--	15
	3.0		--	12	13
	3.5		--	12	16
60%	1.5	1.7	--	11	9
	2.0		--	--	11
	2.5		--	--	12
	3.0		--	--	13
	3.5		--	--	17

\* SMS - Sodium metasilicate solution

† FS - Feed Solution (Ammonium chloride solution)

• TA - Tartaric acid

periods of gel extending from 4 days to 18 days. The maximum length obtained along the growth axis [001] in the case of needle shaped and orthorhombic disphenoidal shaped crystals and along ~~III~~ [101] direction in case of sphenoidal shaped crystals are mentioned. Thus with 1.5M & 2.0% TA length (40 mm) <sup>-long</sup> of needle-shaped crystals were found with progressive reduction in length for orthorhombic disphenoidal and sphenoidal habits i.e. 13 mm of orthorhombic disphenoidal and 7 mm of sphenoidal habit. The table indicates that with a suitable combination of conditions regarding concentration, pH, gel setting time etc. it is possible to grow crystals of desired morphology and size. Table 5.4 presents results with 3M TA of varying quantity & gel pH and fixed quantity of FS of varying concentrations. The table indicates very clearly that optimum conditions can be evolved to grow crystals of desired morphology & size.

#### 5.4 CONCLUSION

From tables 5.3 & 5.4, it is possible to deduce optimum conditions for the growth of good quality crystals of definite morphology. It is understood by the term 'good quality crystals' that the crystals

are geometrically well-developed and are completely transparent. Further the specific gravity of SMS is 1.04, and the ambient temperature 35°C. and quantity 70 c.c. The optimum conditions for different morphologies are as follows :

1. For needle-shaped crystals

- (i) gel pH  $\geq 3$
- (ii) Quantity of TA solution should be 20% of the total solution (SMS + TA) at 35°C.
- (iii) Concentration of FS should be  $\geq 2M$ .

2. For orthorhombic disphenoidal crystals

- (i)  $2 \leq \text{gel pH} \leq 3$ .
- (ii) Quantity of TA solution in the total solution should be between 30% & 40%.
- (iii) Concentration of FS should be between 2M and 3M.

3. For sphenoidal crystals

- (i) gel pH  $\leq 2$
- (ii) Quantity of TA solution  $\geq 40\%$  of the total solution.
- (iii) Concentration of FS should be between 2.4M & 3.5M.

These conditions are true when test tube size is 3.6 c.m. diameter and length 2.0 c.m. The size of a test tube is likely to alter the morphological conditions of the growth of d-AHT crystals. However, this is not studied in detail.



## LIST OF TABLES

- 5.1 Molar concentration of TA (d-tartaric acid) in distilled water at 35°C.
  
- 5.2 Molar concentration of FS (feed solution ammonium chloride) in distilled water at 35°C.
  
- 5.3 Data on crystal morphology, gel pH, molar concentrations of TA for a fixed molar concentration of FS.
  
- 5.4 Data on crystal morphology, gel pH, molar concentration of FS for a fixed molar concentration of TA

CAPTIONS TO THE FIGURES

- 5.1 Schematic drawing of test tube containing
- (a') Rubber cork
  - (a) Ammonium-chloride-Feed Solution (FS)
  - (b) Liquid expelled from gel due to syneresis
  - (c) Crystals on gel-liquid interface
  - (d) Crystals in gel : needle-shaped (N) , orthorhombic disphenoidal (o) and sphenoidal (s)
  - (e) d-tartaric acid impregnated sodium-metasilicate gel.
- 5.2 Photograph of a test tube showing
- (a) Ammonium-chloride-feed solution (FS)
  - (c) Crystals on gel-liquid interface.
  - (d) Crystals in gel : needle-shaped (N), orthorhombic disphenoidal (o) and sphenoidal (s).
  - (e) d-tartaric acid impregnated sodium metasilicate gel.
- 5.3 Photographs of d-AHT crystals of different habits obtained by allowing TA of 3M concentration in a silica gel of sp. gravity 1.04 to react with 2.5M FS.
- (a) 20% TA of gel pH 3.0 to obtain needle-shaped crystals.
  - (b) 40% TA of gel pH 2.2 to obtain orthorhombic disphenoidal.
  - (c) 60% TA of gel pH 1.7 to obtain sphenoidal crystals.

- 5.4 (a,b) Schematic drawing of the (a) bunching of nuclei (shown by lines) (b) subsequent separation into fine needles.
- 5.5 (a) Photograph of bunch-growth of orthorhombic disphenoidal crystals.
- (b) Enlarged portion of bunch-growth (e), shown in (a).
- 5.6 Photograph showing penetration of a growing orthorhombic disphenoidal crystals, in a twinned form (T).
- 5.7 (a) Photograph of growth of twinned sphenoidal crystals in rows (R)
- (b) Enlarged portion of sphenoidal crystals in rows (R) shown in (a).
- 5.8 (a) Photograph of cusp formation around twinned sphenoidal crystals.
- (b) Enlarged portion of cusp around twinned sphenoidal crystals.

CHAPTER - 6

QUANTITATIVE STUDY OF FACTORS  
AFFECTING NUCLEATION & GROWTH  
OF d-AHT

	<u>PAGE</u>
6.1 Introduction   ... ..	111
6.2 Experimental   ... ..	112
6.3 Observations and discussion   ... ..	113
6.3.1 Effect of setting time of gel on morphology of d-AHT crystals	114
6.3.2 Growth of crystal dimensions with gel age   ... ..	116
6.3.3 Effect of concentration of feed solution   ... ..	118
6.3.4 Effect of gel pH   ... ..	121
6.4 Conclusion   ... ..	125
References	



## 6.1 INTRODUCTION

The problem of nucleation is of great importance in practical operation, since a crystal which grows in any particular gel system compete with others for solute. This competition limits their size and perfection and it is obviously desirable to suppress a large number of nucleations until, ideally only one crystal grows in a predetermined location. The available techniques have not yet reached this level of perfection.

The suppression of a large number of nucleation centres is the principal function of the gel, but it is apparent that the degree of suppression ordinarily obtained is insufficient for many of the crystals one wishes to grow. Though ionic diffusion is showed by the soft three dimensional gel frame work, this suppression reaction rate is still larger than the one required for liquid nucleation. Hence nucleation control in a gel medium remains one of the serious problems for a crystal grower. It may be envisaged that the potential nuclei are physically enclosed in gel cells of varying sizes and varying degrees of communication with neighbouring

cells. Gel cell size is influenced by gel density, gel age,<sup>1</sup> (Henisch, 1970) gel pH<sup>2</sup> (Patel and Rao, 1978) and temperature<sup>3</sup> (Nassau et al., 1973). Hence nucleation control can be achieved to some extent by varying these parameters. Other conventional methods such as neutral gel technique<sup>4</sup> (Nickel and Henisch, 1969), seeding,<sup>1</sup> addition of impurities<sup>5,6</sup> (Henisch and Dennis, 1967 ; Barth et al. 1971) have also been employed by some crystal growers. Recently, the growth of single crystals in silica gel media under the influence of an externally applied electric field has drawn the attention of many crystal growers.<sup>7,8</sup> (Suib, 1980 ; Kurian and Ittyachen, 1980) This method is quite promising for a controlled growth of metallic crystals.

In this chapter, influence of several parameters such as gel setting time, gel age, concentration of feed solution, gel pH, concentration of incorporated gel acid, syneresis effect of gel on nucleation and growth of crystals are discussed.

## 6.2 EXPERIMENTAL

The gels were prepared by mixing pure sodium metasilicate solution of known density  $1.04 \text{ gm cm}^{-3}$

with different amounts of d-tartaric acid solution having concentrations from 1.5M to 3.5M as described in section 5.2 (Chapter 5). The pH of the mixture is measured by pH meter. The gel solutions thus prepared were transferred to 3.6 cm diameter and 20 cm long glass test tubes and allowed to set at room temperature which was maintained constant by leaving the test tubes for a number of days in incubator or oven having accuracy of  $\pm 1^{\circ}\text{C}$ . The feed solution, having different concentrations ranging from 1.5M to 3.5M was placed above the set gel for percolation through it and initiation of chemical reaction between FS and TA in the gel under controlled conditions.

### 6.3 OBSERVATIONS AND DISCUSSION

Different parameters such as gel setting time, gel age, gel pH, concentration of feed solution, concentration of incorporated gel acid, etc. which influence directly or indirectly the pore size of a gel were studied to secure optimum conditions for the growth of better quality crystals and also to study the effect of gel syneresis, by which crystals grow on gel surface.

6.3.1 Effect of setting time of gel on morphology  
of d-AHT crystals :

It is now well established<sup>9,10</sup> (Desai and Rai, 1982 ;<sup>Patel</sup> and Venkateswara Rao, 1978) that density of sodium metasilicate solution should be taken as  $1.04 \text{ gm cm}^{-3}$  for preparing a silica gel. Experiments were conducted in the laboratory by different workers to determine appropriate density of SMS<sup>11,12</sup> (Patel 1979 ; Parikh, 1978). It was found from those experiments and others carried out by the present author that the density of SMS solution should be taken as  $1.04 \text{ gm cm}^{-3}$  for preparing tartaric acid impregnated gel. Hence in what follows the density of sodium metasilicate solution would be always  $1.04 \text{ gm cm}^{-3}$ . Setting time of a gel containing different amounts of tartaric acid of varying concentrations is different. The amount of FS and its molar concentration was fixed. This was gently added to set gel. The observations are given in Table 6.1 and graphical plot of setting time of gel in days versus quantity of acid in percentage (20% to 60%) with varying acid concentrations ranging from 1.5M to 3.5M are shown in Figs. 6.1 and 6.2.

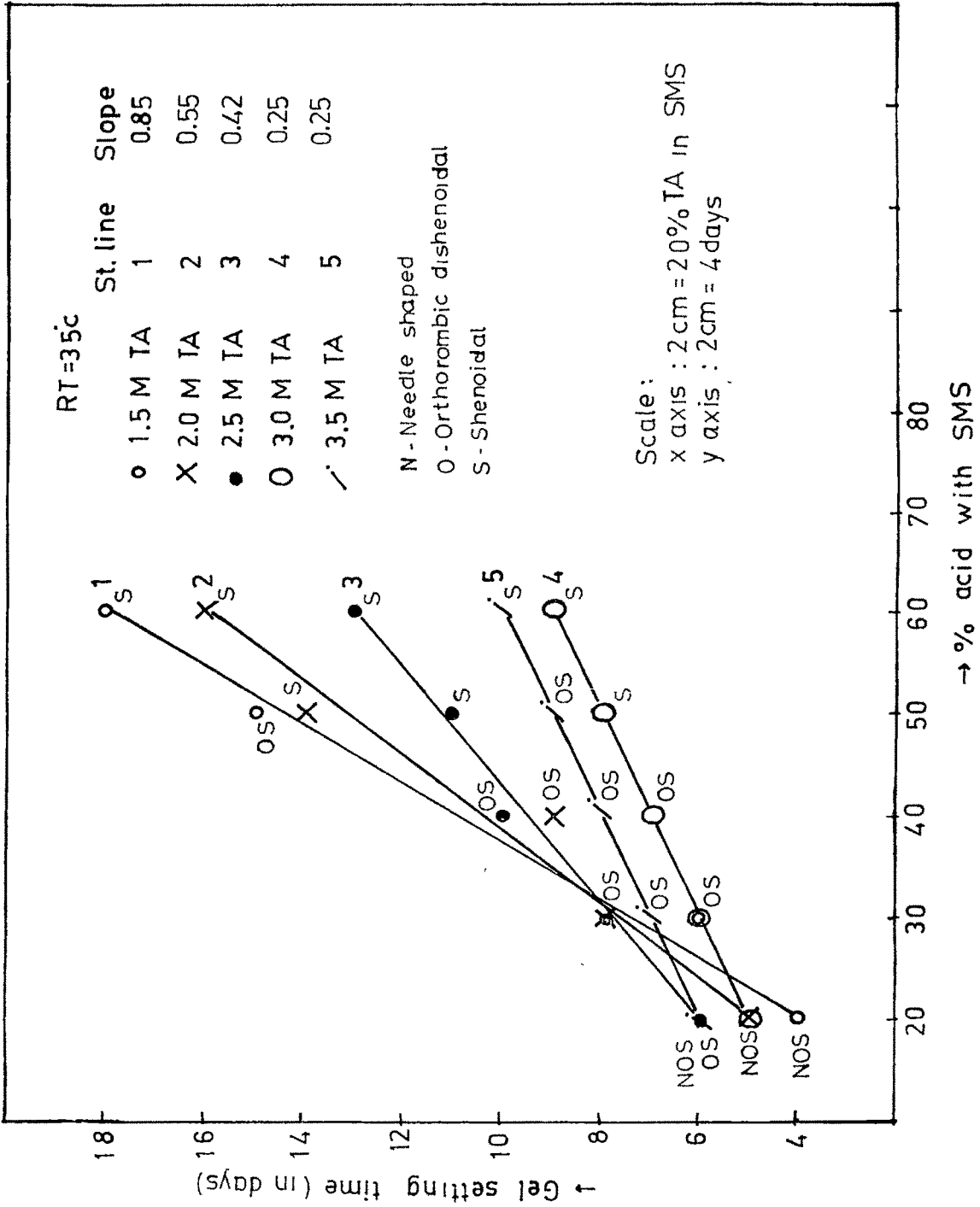


Fig. 6.1

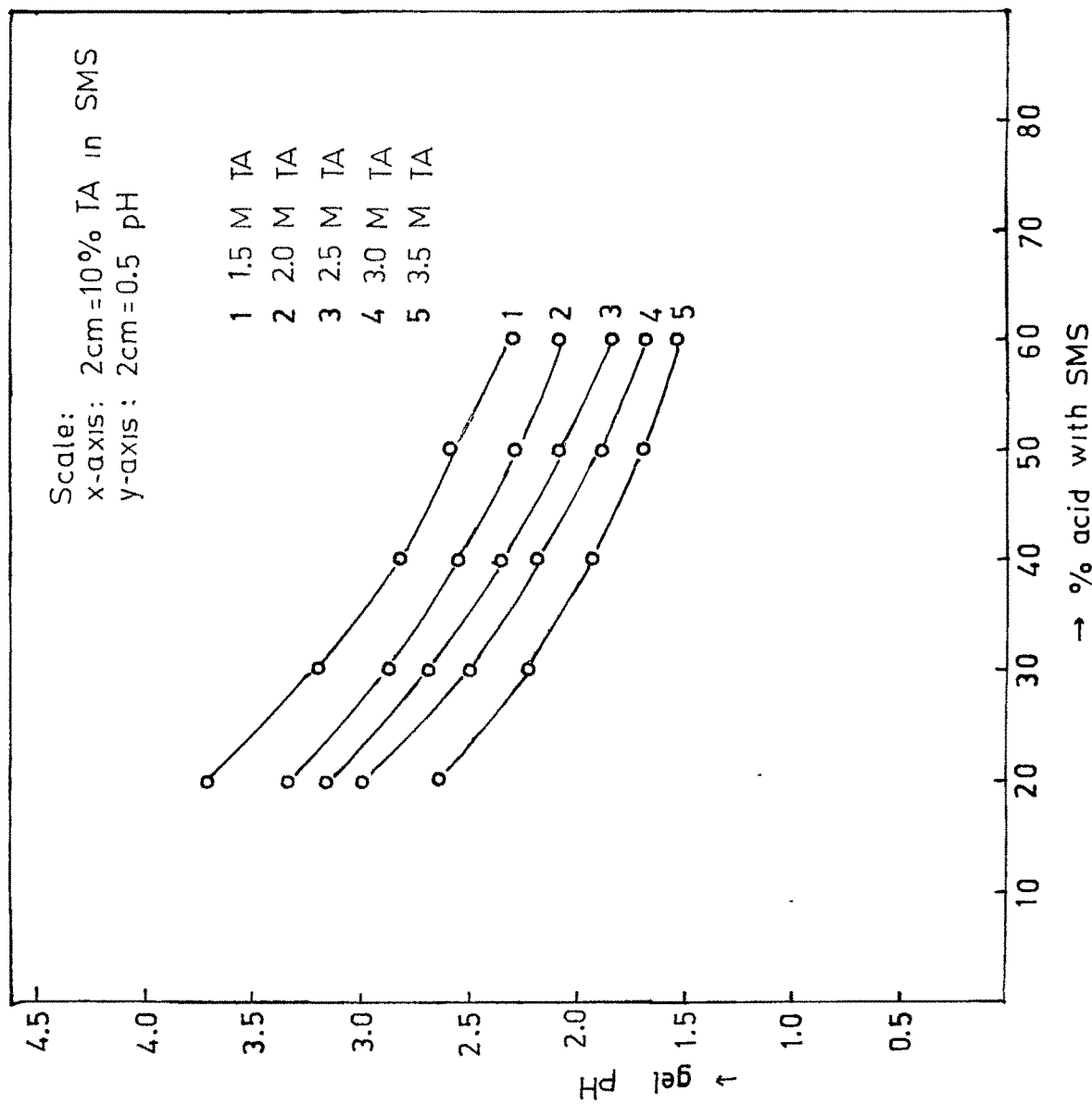


Fig. 6.2

Table - 6.1

Crystal dimension along growth axis, morphology for varying concentration of tartaric acid

R.T. = 35°C  
FS concn = 2M

Conc. of T.A.	% acid with SMS	gel pH	Max. length of crystal			Gel setting time (in days)	slope
			Along -axis Needles (mm)	Along -axis ortho rhombic (mm)	Along 101 sphenoidal (mm)		
	P				T	T/P	
1.5M	20%	3.72	40	13	7	4	
	30%	<u>3.2</u>	--	16	10	6	
	40%	2.82	--	31	7	10	0.85
	50%	2.51	--	16	10	15	
	60%	<u>2.30</u>	--	--	8	18	
2.0M	20%	3.36	36	12	--	5	
	30%	2.87	--	16	8	8	
	40%	2.56	--	--	14	9	0.55
	50%	<u>2.3</u>	--	--	13	14	
	60%	<u>2.1</u>	--	--	11	16	

Table cont...

Table 6.1 cont....

2.5M	20%	<u>3.18</u>	31	13	-	6
	30%	2.70	--	16	8	8
	40%	2.37	--	17	9	10
	50%	2.09	--	--	9	11
	60%	1.85	--	--	10	13
3.0M	20%	3.00	56	14	-	5
	30%	2.50	--	22	6	6
	40%	2.2	--	17	8	7
	50%	1.9	--	--	10	8
	60%	1.7	--	--	11	9
3.5M	20%	2.65	--	22	7	6
	30%	2.25	--	10	10	7
	40%	1.95	--	14	12	8
	50%	1.73	--	14	9	9
	60%	1.56	--	--	12	10

\* Identical gel pH values (underlined) for different molar concentrations of T.A.

In Fig. 6.1 straight line plots of gel setting time in days versus quantity of acid in gel for varying concentrations of acid are given. Some salient features of the plots are as follows :

- (1) Needle-shaped, orthorhombic disphenoidal and sphenoidal crystals are obtainable at 20% quantity of acid, irrespective of gel pH.
- (2) For 30% and 40% quantity of acid, only orthorhombic disphenoidal and sphenoidal crystals are obtainable.
- (3) The sphenoidal crystals are obtainable for 50% and 60% quantity of acid.
- (4) It is also clear from the plots that gelation time varies in inverse proportion with gel pH at a given temperature. Greater is the gelation time, larger is the gel pH and conversely (Fig. 6.2).
- (5) For concentrated acid in gel, the variation of gelation time with quantity of acid in percentage in SMS solution is less, as can be

seen from the slopes of these straight line plots (Fig. 6.1). The slopes which represent gel setting time in days per unit percentage of TA in SMS for a given acid, pH decreases with increase in concentrations of TA and based on the experimental observations that gel setting time required for saturated solution of TA is constant for different quantities of acid in gel, It can be concluded that the slope should be almost zero for the saturated solution.

It is rather remarkable that it is the quantity of acid in gel and not the gel pH which is solely responsible for the crystal habits. This conclusion is also supported by photographs 6.3 a,b,c, which depict growth of d-AHT, obtained from a chemical reaction between 3M tartaric acid in gel (70 c.c. mixture) and 2.5M ammonium chloride (70 c.c.) with varying quantity of acid 20%, 40% and 60%.

### 6.3.2 Growth of crystal Dimensions with gel age

It is shown above that all habits of d-AHT crystals are observable when the quantity of tartaric

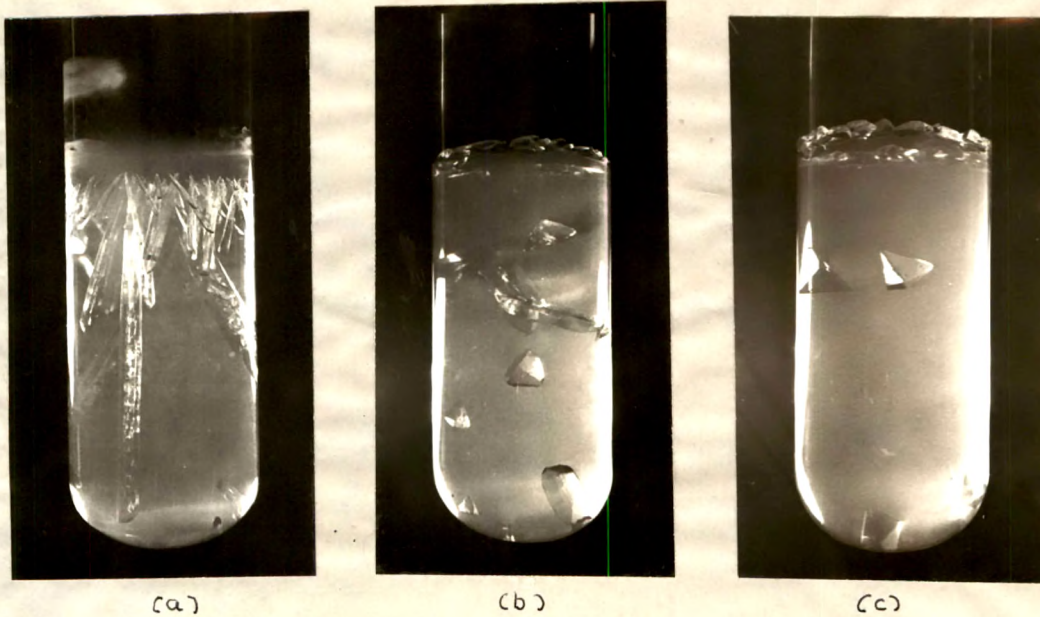


Fig. 6.3 Photographs of d-AHT crystals of different habits obtained by 3M TA incorporated gel reacted with 2.5M FS

- (a) 20% TA of gel pH 3.0 to obtain needle-shaped crystals
- (b) 40% TA of gel pH 2.2 to obtain orthorhombic disphenoidal and sphenoidal crystals.
- (c) 60% TA of gel pH 1.7 to obtain sphenoidal crystals.

acid in gel was 2.0%. Since the length of needle-shaped crystal is maximum (56 mm) at gel pH 3 (table 6.1). SMS gel impregnated with 2.0% TA (of 3M concn) and FS of 2M concentration was used in the present experiment (R.T. 33°C). In order to determine the effect of gel age on crystal dimensions, travelling microscope with a least count of 0.001 cm was employed. Of all the habits, needle-shaped crystals were easily amenable for measurement along the vertical direction of growth.

The set gel was aged in a regular manner. After a certain age fixed quantity of FS (of 2.5M concn) was gently added to the gel surface to initiate a chemical reaction between FS and gel acid. The observations of time (gel age), length along the growth axis and growth rate for different gel ages at room temperature (33°C) are given in table 6.2. The variation of linear dimension of needle-shaped crystals along the vertical C-axis with time for various gel ages are graphically studied (Fig. 6.4a,b). It is clear from the plots that the growth of needle-shaped crystals increases with the time of arrival of feeding material to the crystal, attains an optimum value and remains

RT - 33° C TA concn = 2.5M Growth Rate of Needle shaped Crystals for different gel ages  
20% acid gel FS concn = 2.5M

Time in Hours	1 day gel		2 days gel		3 days gel		4 days gel		5 days gel	
	Length in cm	Growth rate -l cm hr	Length in cm	Growth rate -l cm hr	Length in cm	Growth rate -l cm hr	Length in cm	Growth rate -l cm hr	Length in cm	Growth rate -l cm hr
0.5	0.101	0.202	0.115	0.232	0.100	0.200	0.245	0.409	0.209	0.418
1.0	0.252	0.252	0.211	0.211	0.249	0.249	0.395	0.395	-	-
1.5	0.365	0.243	0.349	0.233	0.301	0.201	0.480	0.320	0.299	0.199
2.0	0.503	0.252	0.470	0.235	0.491	0.246	0.551	0.276	0.404	0.202
2.5	0.550	0.220	0.531	0.192	0.542	0.217	0.575	0.230	0.500	0.200
3.0	0.600	0.200	0.490	0.163	0.580	0.193	0.591	0.197	0.543	0.181
3.5	0.655	0.187	0.501	0.143	0.614	0.175	0.601	0.172	0.592	0.169
4.0	0.703	0.176	0.511	0.128	0.629	0.157	0.616	0.154	0.640	0.160
4.5	-	-	-	-	0.650	0.144	-	-	0.704	0.156
5.0	0.780	0.156	0.511	0.102	0.681	0.136	0.648	0.130	0.773	0.155
6.0	0.841	0.140	0.511	0.085	0.725	0.121	0.684	0.114	0.804	0.134
7.0	0.892	0.127	-	-	0.782	0.112	0.692	0.099	0.804	0.115
8.0	0.930	0.116	0.511	0.064	0.818	0.102	0.750	0.094	0.809	0.101
9.0	0.942	0.105	-	-	-	-	-	-	-	-
10.0	0.950	0.095	-	-	-	-	-	-	-	-
11.0	0.953	0.087	-	-	-	-	-	-	-	-
12.0	0.955	0.080	-	-	-	-	-	-	-	-
22.0	0.980	0.045	0.511	0.023	0.923	0.042	-	-	0.829	0.038
24.0	0.980	0.041	0.511	0.021	0.930	0.039	0.800	0.033	0.829	0.035

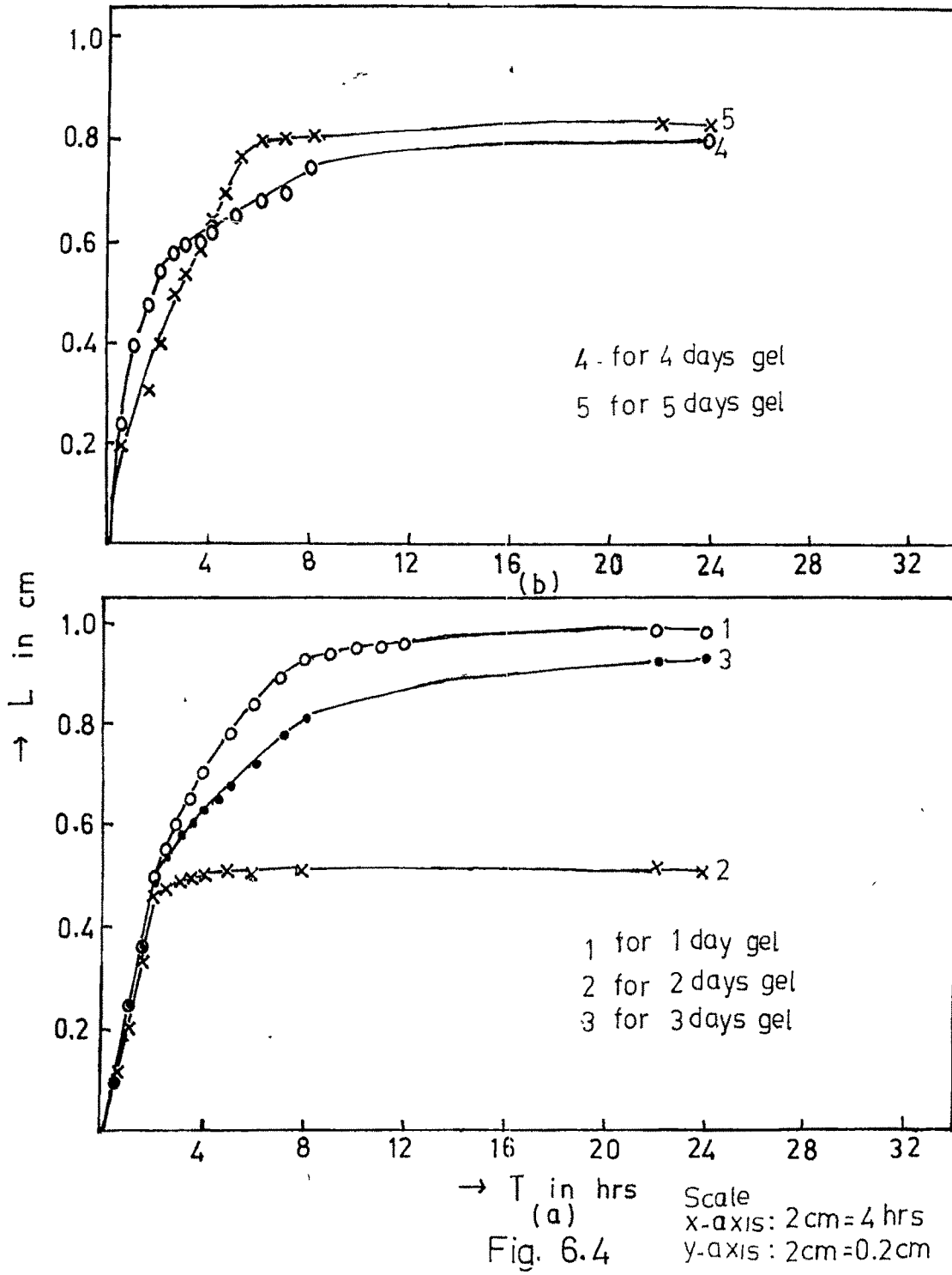


Fig. 6.4

practically constant. The growth slows down after 8 hours or so, this is indicated by the curvature in the plot. Further the results indicate that so far as the gel remains wet and free from fungus formation, the gel age does not affect the growth significantly, as can be seen from the growth rates (tables 6.2). Identical conclusions were obtained for the variations of lateral dimensions of crystal with gel age.

### 6.3.3 Effect of Concentration of Feed Solution

FS solutions with concentrations varying from 1.5M to 3.5M were prepared. It is clear from table 6.1 that for the same molar concentration of TA, gel pH depends on the quantity of TA and gelation time e.g. for gel pH 2.3, underlined in the table, for 60% quantity of TA, gelation time 18 days, the molar concentration of TA is 1.5M, whereas for the same gel pH (2.3), molar concentration (2M) and the quantity of TA (50%), the gel setting time is 14 days. Hence in the present experiment with fixed gel pH, different concentrations and quantity of TA and gelation time were taken. Alternatively with fixed concentration of TA, quantity

of TA and gelation time were chosen for obtaining the desired gel pH. Density of SMS was  $1.04 \text{ gm/cm}^3$ . Different amounts of TA in gel varying from 20 to 60% were taken. The gel pH was measured in the usual way. FS of different concentrations were gently added to the set gel for studying effect of FS concentration on nucleation. <sup>(Table 6.3)</sup> The results are shown graphically by plotting the number of crystals per unit volume of gel at the gel interface and also inside the gel versus FS concentrations for different values of gel pH. The significant points for these graphs are as follows :

- (i) Due to syneresis, crystals grow on gel, surface and maximum number of crystals per unit volume are indicated by extremum points C and D (Fig. 6.5a) for gel pH 1.7 and 2.2, respectively. On either side of these values, the variation of number density with concentration is almost linear.
- (ii) Inside the gel the variation of number density with FS concentration is almost linear. Linear character is more sharp for gel pH 1.7 at which the concentration of feed solution is not having any noticeable effect on number density (Fig. 6.5b).

T A B L E 1 6.3  
\*\*\*\*\*

Data on number density of d - AHT Crystals and their weights for varying concentrations of FS and gel PH

% of T A with S M S	gel PH	Concentration of FS (in M)	Crystals at interface		Total crystals in test tube		Wt. of Crystals grown at interface		Wt. of Crystals grown in gel		R.T = 35° C TA concn = 3M Wt. of crystals grown in test tube T = a + b (mg per Cm <sup>3</sup> )
			a	b	N per Cm <sup>3</sup>	T = a + b N per Cm <sup>3</sup>	(mg per Cm <sup>3</sup> )	(mg per Cm <sup>3</sup> )	(mg per Cm <sup>3</sup> )	(mg per Cm <sup>3</sup> )	
20%	3.00	1.5	0.0	0.28	0.28	0.0	0.0	34.6	34.6	34.6	34.6
		2.0	0.0	0.66	0.66	0.0	0.0	40.6	40.6	40.6	40.6
		2.5	0.0	0.83	0.83	0.0	0.0	42.7	42.7	42.7	42.7
		3.0	0.0	1.38	1.38	0.0	0.0	44.1	44.1	44.1	44.1
		3.5	0.0	1.80	1.80	0.0	0.0	44.8	44.8	44.8	44.8
30%	2.50	1.5	0.15	0.09	0.24	8.6	20.6	20.6	30.5	30.5	30.5
		2.0	0.38	0.23	0.61	5.7	31.4	31.4	37.1	37.1	37.1
		2.5	0.15	0.31	0.46	2.0	40.1	40.1	40.8	40.8	40.8
		3.0	0.0	0.31	0.31	0.0	42.1	42.1	42.7	42.7	42.7
		3.5	0.0	0.51	0.51	0.0	46.1	46.1	46.1	46.1	46.1
40%	2.20	1.5	0.26	0.09	0.35	10.3	12.4	12.4	22.7	22.7	22.7
		2.0	0.58	0.20	0.78	7.8	23.1	23.1	30.8	30.8	30.8
		2.5	0.50	0.16	0.66	8.4	26.3	26.3	34.7	34.7	34.7
		3.0	0.70	0.22	0.92	5.6	31.7	31.7	37.3	37.3	37.3
		3.5	0.77	0.34	1.1	2.3	36.9	36.9	39.2	39.2	39.2
50%	1.90	1.5	0.30	0.08	0.38	10.4	7.8	7.8	18.2	18.2	18.2
		2.0	0.63	0.14	0.77	15.8	9.8	9.8	25.4	25.4	25.4
		2.5	0.70	0.08	0.78	9.7	20.3	20.3	30.0	30.0	30.0
		3.0	0.59	0.16	0.76	6.9	24.6	24.6	31.5	31.5	31.5
		3.5	1.13	0.11	1.24	3.5	31.1	31.1	34.6	34.6	34.6
60%	1.70	1.5	0.22	0.01	0.23	10.4	2.0	2.0	12.4	12.4	12.4
		2.0	0.69	0.07	0.76	6.8	12.7	12.7	19.5	19.5	19.5
		2.5	0.49	0.07	0.55	12.6	12.5	12.5	25.1	25.1	25.1
		3.0	0.77	0.08	0.85	6.3	20.1	20.1	26.3	26.3	26.3
		3.5	0.92	0.05	0.97	3.2	27.5	27.5	30.7	30.7	30.7

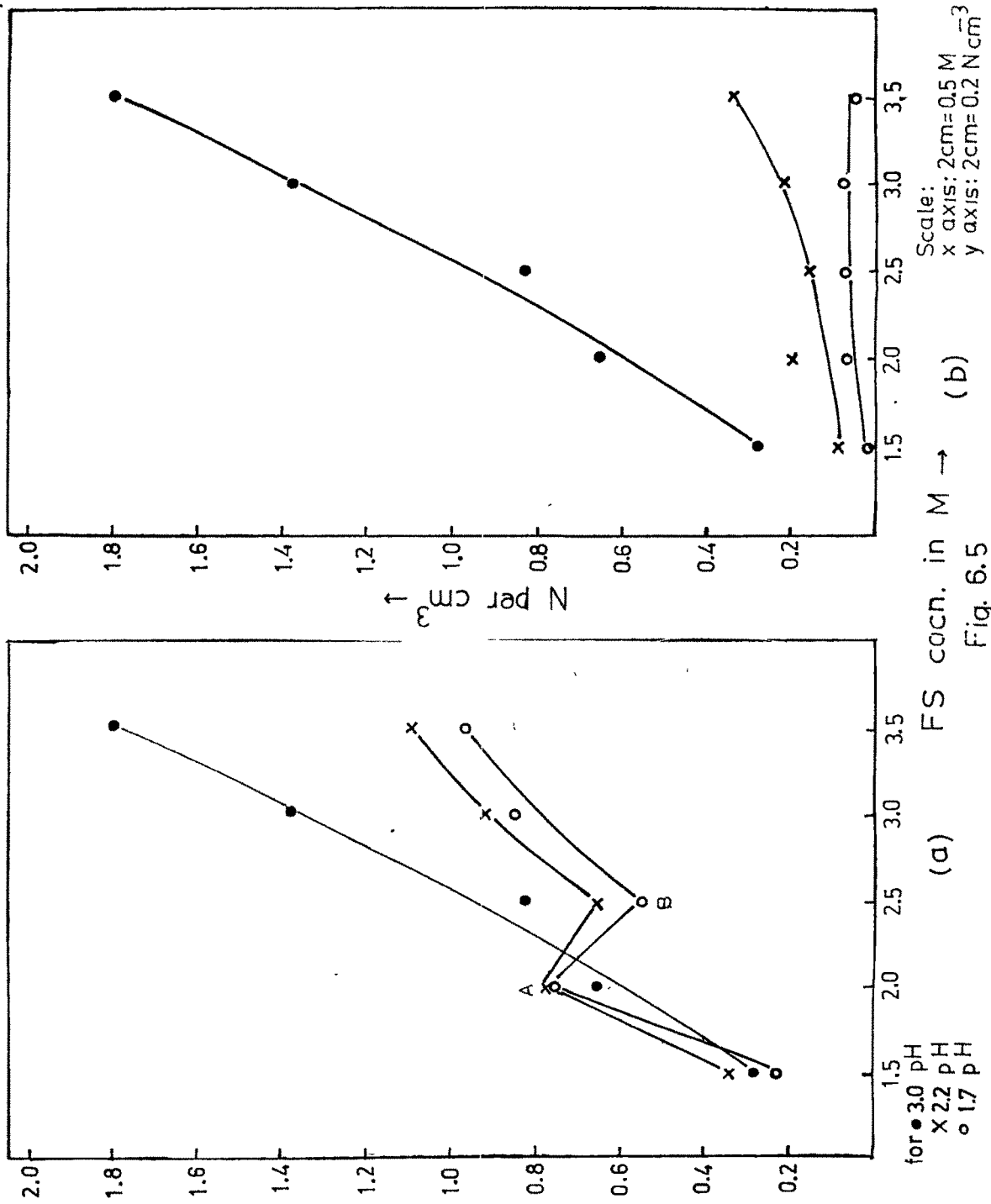


Fig. 6.5

- (iii) Combination of visual inspection of crystals growing in a gel and careful study of plots show that pH values 1.7 and 2.2 and concentration range 1.5 to 2.5M of FS are useful for obtaining transparent crystals. Beyond 2.5M concentration, (Fig. 6.6a,b) the size of the needle shaped crystal increases and the number of translucent crystals are is more than the number of transparent crystals, whereas for sphenoidal crystals (6.7a,b) the size does increase with more number of transparent crystals and less number of translucent crystals. This is obviously influenced by gel pH and the availability of quantity of gel acid.
- (iv) Incidentally comparison of plots of Fig. 6.5a and 6.5b provide valuable information about the useful molar concentrations of FS, namely 2.0 and 2.5M in the gel growth of d-AHT. This shows that while considering growth of good quality crystals phenomenon of syneresis has to be carefully considered.

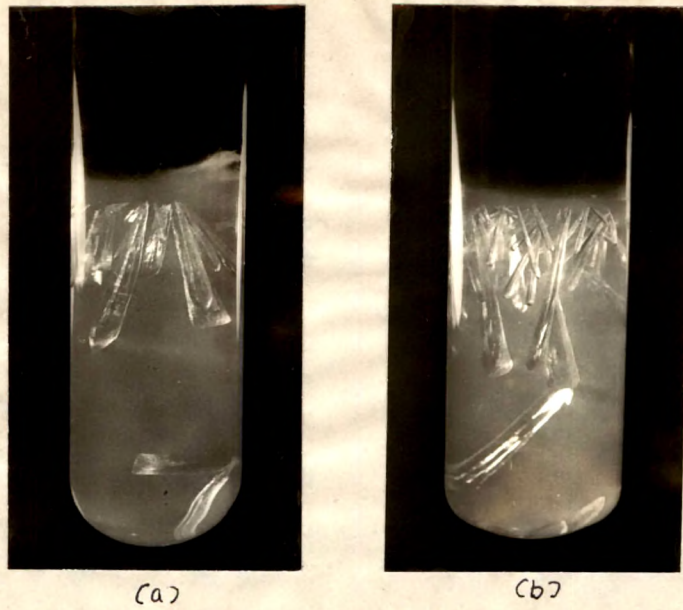


Fig. 6.6 Photograph of test tubes showing needle-shaped d-AHT crystals formed by using 2.5M TA with (a) 2.5M FS (b) 3.5M FS, showing the increase in the number of crystals with FS concentration.

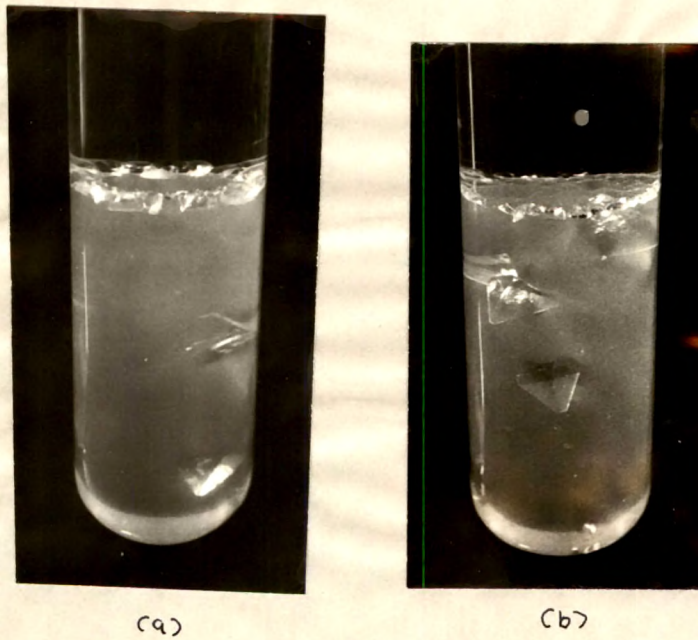


Fig. 6.7 Photograph of test tubes showing sphenoidal d-AHT crystals formed by using 2.5M TA with (a) 3.0M FS and (b) 3.5M FS showing the increase in the number of crystals with FS concentration.

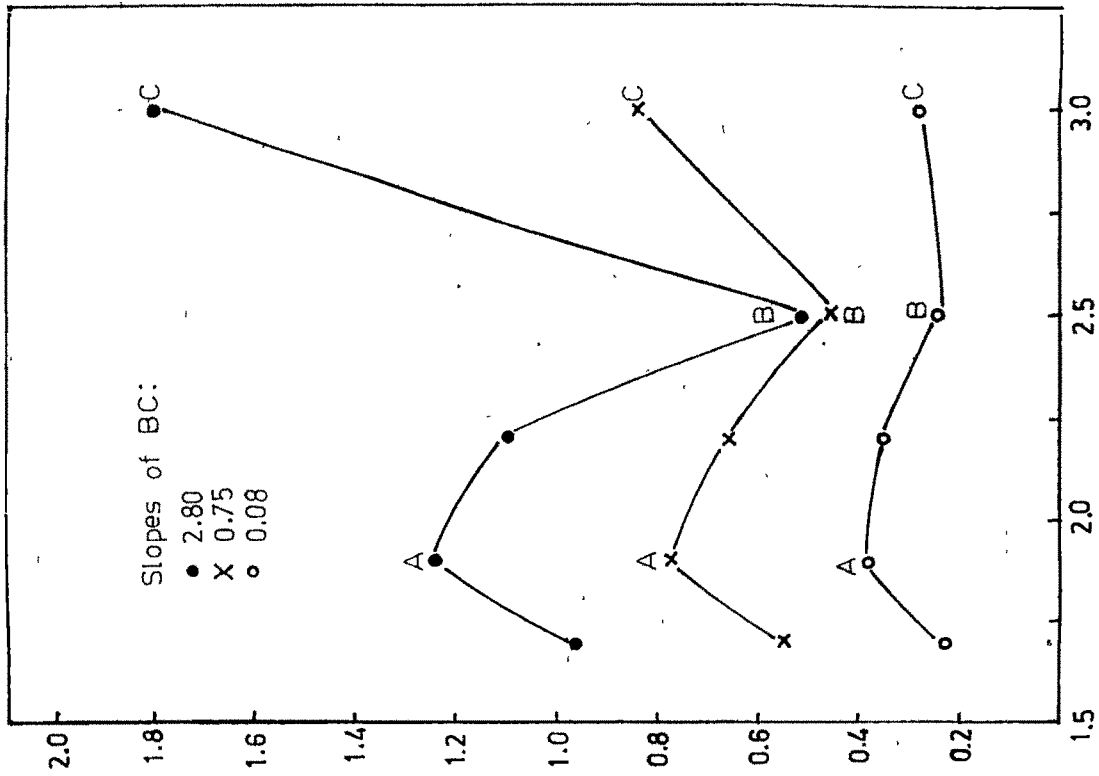
#### 6.3.4 Effect of Gel-pH

It is known that pH of a gel is associated with its pore size ; larger is the pore size in a gel, smaller is its pH value<sup>1</sup>. Pore size in turn controls the intake of chemicals taking part in a reaction in pore volume. This produces different crystallographic habits of crystal.<sup>13</sup> Typical experimental set up and observations are shown in table 6.3. In all cases gel pH was determined at the time of mixing gel solutions and feed solution is added on surface of a set gel in a test tube. Fig. 6.3a exhibits noticeable growth of d-AHT crystals along the vertical direction parallel to tube walls. Since the lateral growth is comparatively insignificant mostly needle-shaped crystals are formed. The growth took place when gel pH was 3 or more. In Fig. 6.3b the top portion of the gel in the tube consists of orthorhombic disphenoidal crystals whereas central and bottom part near the corner exhibit a number of well-developed sphenoidal crystals. One crystal at the bottom is orthorhombic disphenoidal, which is likely to be due to slipping of FS near tube wall. When gel pH is in between 2 and 3 the orthorhombic disphenoidal and sphenoidal

crystals are obtainable. Fig. 6.3 shows the growth of sphenoidal crystals. This habit is obtainable when gel pH is less than 2. Since larger pH value corresponds to a loosely bound platelet structure of gel, crystals in the form of needles are obtained. At such gel pH value crystals are found to be translucent and not well defined. As pH of the gel decreases, the box-like network structure takes place,<sup>1</sup> (Henisch, 1970) the diffusion of feed-solution is slow<sup>14</sup> and as a result the trapping of molecules by crystal nuclei is less under these conditions sphenoidal crystals are observed. These conclusions are in tune with those observed in the earlier chapter. Fig. 6.8a,b are the plots of the number of crystals perunit volume of gel at the gel interface and also inside the gel versus gel pH for a few concentrations of FS (1.5M, 2.5M and 3.5M).

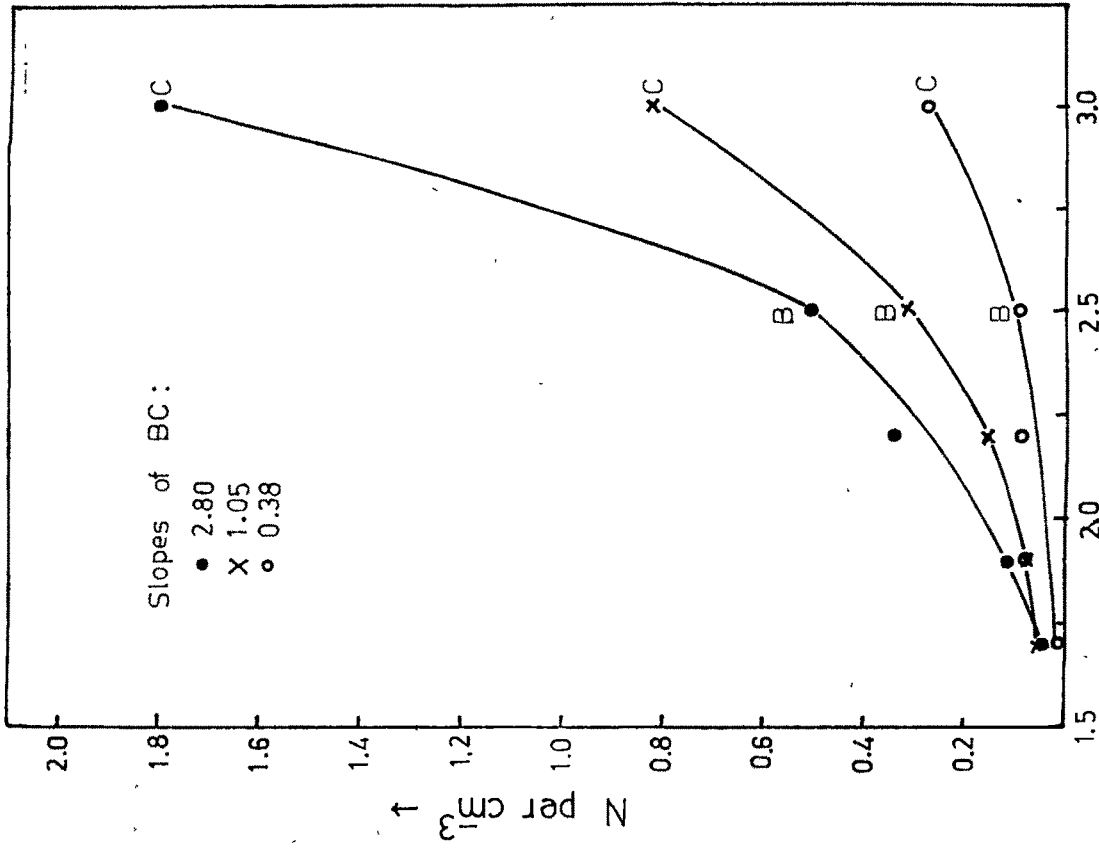
The following points are noticeable :

- (i) The plot (6.8a) exhibit extremum points A & B for gel pH 1.9 and 2.5 respectively. These points indicate different habits of d-AHT crystals, namely sphenoidal and orthorhombic disphenoidal and sphenoidal (Figs. 6.3c and 6.3b).



Scale: 2cm=0.25 pH  
X axis: 2cm=0.2 N cm<sup>-3</sup>  
Y axis: 2cm=0.2 N cm<sup>-3</sup>

(a)



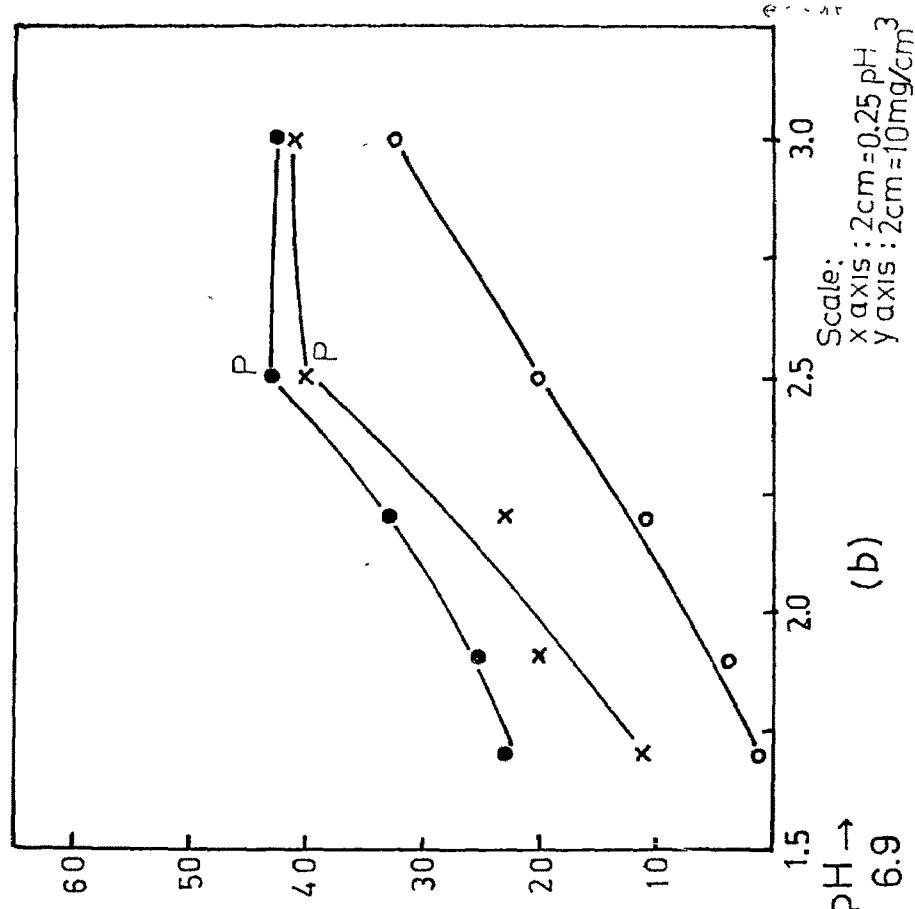
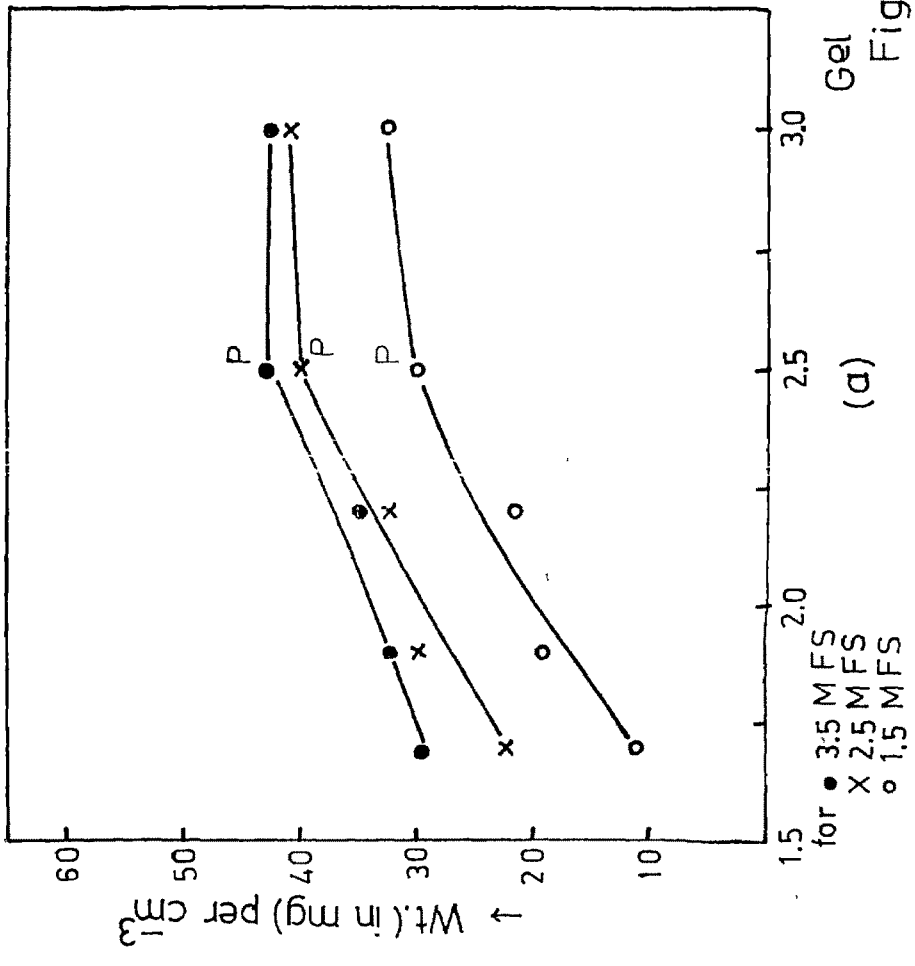
Scale: 2cm=0.25 pH  
X axis: 2cm=0.2 N cm<sup>-3</sup>  
Y axis: 2cm=0.2 N cm<sup>-3</sup>

(b)

Fig. 6.8

of acid liberated on gel top and associated with pores inside gel with feed solution. The plots of weight of grown crystals per unit gel volume of total crystals grown in test tube and inside the gel with gel pH are shown in Fig. 6.9a,b. The noticeable features of these plots are as follows :

- (i) The total weight increases non-linearly with gel pH and molar concentration of FS (Fig. 6.9a).
- (ii) At 2.5 gel pH a turning point P is noticeable, except for plot corresponding to 1.5M of FS. (Fig. 6.9b).
- (iii) After the above pH value, the weight remains almost constant with increase of pH. This is found to be true for all concentrations of FS.
- (iv) For lower gel pH, number of nuclei inside the gel is less (Fig. 6.8a,b). This is true for higher FS concentration, whereas weight of crystals increases noticeably with FS concentration at lower gel pH. The crystals are of bigger size with increase of FS concentration. (Fig. 6.7b, 6.8b).



Scale:  
 X axis : 2cm = 0.25 pH  
 Y axis : 2cm = 10mg/cm<sup>3</sup>

(a) (b)  
 Fig. 6.9

In the earlier cases the number of crystals per unit volume of gel (i) grown inside the gel and (ii) grown at different parts of the gel and also at the gel interface versus gel pH for different FS concentrations were graphically studied. It is also desirable to determine the number of crystals at the gel interface only, i.e. those crystals which were formed due to chemical reaction between FS and the expelled acid. Fig. 6.10 represent typical plots for the number density versus gel pH for different FS concentrations (1.5M, 2.5M and 3.5M). All these plots exhibit maximum number of crystals at a certain gel pH 1.9 and less number of crystals on either side of these maxima. This value of gel pH is almost the same as that shown in Fig. 6.8a, indicating that syneresis phenomenon has to be considered while discussing the effects of other parameters mentioned above.

#### 6.4 CONCLUSION

The quantitative study of various gel parameters on nucleation and growth of d-AHT crystals has clearly shown that

- (i) quantity of acid in gel has a dominating effect on the morphology of d-AHT crystals.

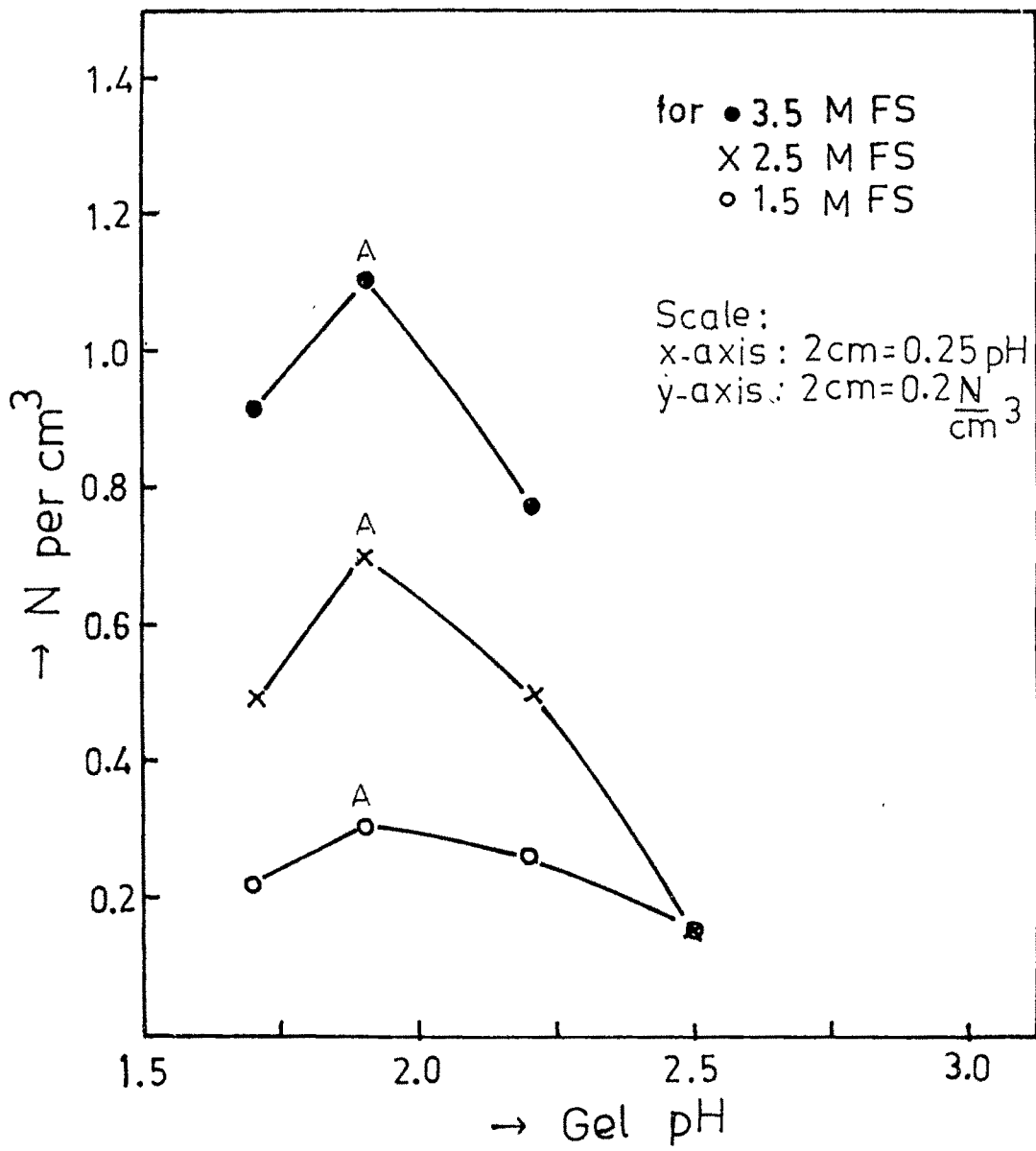


Fig. 6.10

- (ii) For a wet and fungusfree gel, the gel age does not noticeably affect crystal growth.
  
- (iii) While considering the effect of concentration of FS and of gel pH on the number of grown crystals per unit volume of gel, the phenomenon of syneresis has to be carefully considered for obtaining useful information about FS concentration and gel pH.
  
- (iv) The above conclusions fairly agree with those obtained in chapter 5 on the qualitative study of growth of d-AHT crystals of different habits.



- |     |   |      |  |
|-----|---|------|--|
| 8.  | KURIAN, K.V.<br>and ITTYACHEN,<br>M.A.                        | 1980 | J. Mat. Science<br>15, 1724.   |
| 9.  | DESAI, C.C. and<br>RAI, J.A.                                  | 1987 | Surface technology,<br><u>15</u> , 131   |
| 10. | PATEL, A.R. and<br>VENKATESWARA<br>RAO, A.                    | 1978 | J. of Crystal<br>Growth <u>43</u> , 351.   |
| 11. | PATEL, S.M.   | 1979 | M.Sc. (Applied<br>Physics) Desertation,<br>M.S. University of<br>Baroda, Baroda. |
| 12. | PARIKH, A.S.  | 1978 | M.Sc. (Applied<br>Physics) Desertation,<br>M.S. University of<br>Baroda, Baroda. |
| 13. | ALEKSANDRZYK, K ;<br>WIKTOROWSKA, B.<br>and WOJCIECHOWSKI, B. | 1981 | J. of crystal<br>growth, <u>52</u> , 868.  |
| 14. | PILLAI, K.M. and<br>ITTYACHEN, M.A.                           | 1978 | Praman, <u>10</u> , 6,<br>613  |

## List of Tables

- 6.1 Crystal dimension along growth axis, morphology for varying concentrations of tartaric acid.
- 6.2 Growth rate of needle-shaped crystals for different gel ages.
- 6.3 Data on number density of d-AHT crystals and their weights for varying concentrations of FS and gel pH.

### Captions to the Figures

- 6.1 Plot of gel setting time (T) in days versus percentage of acid (TA) in SMS for different concentrations of TA and different crystal habits needle-shaped (N), orthorhombic disphenoidal (o) and sphenoidal (s)
- 6.2 Plot of gel pH (initial value of pH of a mixture of TA + SMS) versus percentage of acid (TA) in SMS.
- 6.3 Photographs of d-AHP crystals of different habits obtained by 3M TA incorporated gel reacted with 2.5M FS
- (a) 20% TA of gel pH 3.0 to obtain needle-shaped crystals
- (b) 40% TA of gel pH 2.2 to obtain orthorhombic disphenoidal and sphenoidal crystals.
- (c) 60% TA of gel pH 1.7 to obtain sphenoidal crystals.

- 6.4(a,b) Plots of growth of needle-shaped crystals for different gel-ages.
- 6.5(a,b) Plots of number of crystals per unit volume of gel for (a) total crystals growth at interface and in gel (b) crystals grown in gel versus concentration of FS, for different gel pH.
- 6.6(a,b) Photograph of test tubes showing needle-shaped d-AHT crystals formed by using 2.5M TA with (a) 2.5M FS (b) 3.5M FS, showing the increase in the number of crystals with FS concentration.
- 6.7(a,b) Photograph of test tubes showing sphenoidal d-AHT crystals formed by using 2.5M TA with (a) 3.0M FS and (b) 3.5M FS showing the increase in the number of crystals with FS concentration.
- 6.8(a,b) Plots of number of crystals per unit volume of gel for (a) total crystals grown at interface and in gel (b) crystals grown in gel versus gel pH, for different FS concentration.

6.9(a,b) Plots of weight of crystals per unit volume of gel for (a) total crystals grown at interface and in gel (b) crystals grown in gel versus gel pH, for different ES concentrations.

6.10 Plots of number of crystals grown at interface per unit volume of gel versus gel pH for different ES concentrations.

CHAPTER - 7

CHARACTERIZATION OF GEL GROWN

d-AHT

	<u>PAGE</u>
7.1 Introduction ... ..	127
7.2 Chemical Analysis .. ...	127
(a) Analysis for Carbon and Hydrogen ..	128
(b) Analysis for Nitrogen ... ..	129
(c) Estimation of oxygen ... ..	130
(d) Calculated percentage ... ..	131
7.3 X-ray diffraction method ... ..	132
7.3.1 Determination of lattice parameters .....	132
7.3.2 Laue method .....	141
7.4 Indices of the grown faces ... ..	142
7.4.1 Stereographic projection of d-AHT ... ..	142
7.4.2 Miller indices for natural habit faces of d-AHT crystal ..	150
7.5 Specific rotation .....	155
7.6 Specific gravity of crystal .. ...	157

References

\*\*\*\*\*  
\*\*\*\*\*  
\*\*\*\*\*  
\*\*\*\*\*  
\*\*\*\*\*

## 7.1 INTRODUCTION

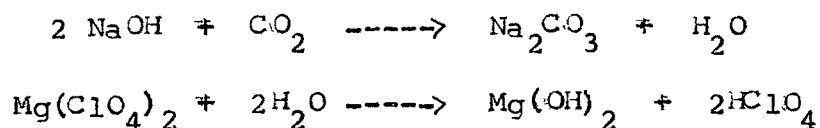
Ammonium-hydrogen-d-tartrate (d-AHT) crystals grown by gel method (cf. Chapter 5) are characterised by different chemical and physical methods. Quantitative chemical analysis was used to check the chemical constitution and x-ray diffraction technique was used to determine lattice parameters. The single crystalline character was tested by etch method and <sup>Laue</sup> ~~have~~ diffraction method. Other physical properties such as optical activity, density, hardness, etc. were also determined.

## 7.2 CHEMICAL ANALYSIS :

Microchemical analysis was carried out to determine elemental content present in d-AHT  $(\text{NH}_4 \cdot \text{H} \cdot \text{C}_4 \text{H}_4 \text{O}_6)$  crystals. Fairly big size d-AHT crystal was selected and it was cut into two parts, one part was used for determination of carbon and hydrogen and the other was used for deciding content of nitrogen by Dumas's method. Carbon, hydrogen, nitrogen and oxygen atoms were found to be present, by the following quantitative method.

## (a) Analysis for Carbon and Hydrogen :

Carbon and hydrogen estimation was carried out by Paigal standard method<sup>1</sup> (Hendrickson et al. 1970) using Coleman C-H analyzer. A weighed portion of the compound was burned in oxygen, over hot copper oxide at about 700°C. Carbon dioxide and water vapour were produced and were individually captured and weighed in absorption tubes. For CO<sub>2</sub>, the reagent used for adsorption was sodium hydroxide coated over soda asbestos, and magnesium perchlorate Mg(ClO<sub>4</sub>)<sub>2</sub> was used for water. The chemical reactions taking place were as under :



In the present case, the amounts of sample taken and those collected of CO<sub>2</sub> and H<sub>2</sub>O were as under :

Amount of sample (d-AHT) used	=	5.650 mg
Amount of CO <sub>2</sub> collected	=	6.074 mg
Amount of H <sub>2</sub> O collected	=	2.554 mg

From these values, the percentage of C & H in the sample present were found to be

$$\% \text{ C} = 29.31 \%$$

$$\% \text{ H} = 5.055 \%$$

(b) Analysis for Nitrogen :

Dumas analysis was used to determine the percentage of nitrogen. The sample (d-AHT) was mixed with cupric oxide ( $\text{CuO}$ ) and was heated to a dull-red heat, which resulted in complete oxidation of the organic material. The resulting gases were passed over a surface of hot copper to reduce nitrogen oxide to nitrogen. The other more active gases (chlorine, ozone, carbon dioxide etc.) were chemically absorbed and the residual volume of nitrogen was measured carefully at definite temperature and pressure. The weight of nitrogen was calculated (by ideal gas law) and was divided by the initial sample weight to give the fraction of nitrogen in the original compound.

The nitrogen content in the sample was found to be as under :

Initial weight of sample (d-AHT) = 5.089 mg

Vol. of nitrogen collected = 0.3659 ml

By a calculation

$$\% \text{ N observed} = 7.957 \%$$

(c) Estimation of oxygen :

By the stoichiometric principles of general chemistry<sup>1</sup> (Hendrickson, 1970), the sum of percentages of components equals approximately 100 per cent. The sum of the percentages of C, H and N was found to be  $(29.31 + 5.055 + 7.957) 42.322$ , which is less than 100. This means that oxygen is present in the compound.

$$\begin{aligned} \% \text{ oxygen} &= 100 - 42.322 \\ &= 55.678\% \end{aligned}$$

The above percentage value of oxygen also includes the impurities inherently present in the reacting chemicals, namely ammonium chloride and d-tartaric acid, which contains permissible impurities given by the manufacturers (Table 7.1 and 7.2). As a matter of fact, this

Table 7.1

Ammonium Chloride (G.R.) ( $\text{NH}_4\text{Cl}$ )

Sarabhai M. Chem., Baroda, India

Assay	min	99.8%
pH value (5% aq. soln)		4.5 to 5.5
Insoluble portion	max	0.001 %
Residue on ignition (as $\text{SO}_4$ )	max	0.005 %
Arsenic (As)	max	0.00005 %
Calcium (Ca)	max	0.001 %
Copper (Cu)	max	0.00025%
Iodide (I)	max	0.001%
Iron (Fe)	max	0.0002%
Heavy metals (as Pb)	max	0.000 <sup>2</sup> <sub>5</sub> %
Nitrate ( $\text{NO}_3$ )	max	0.00005 %
Phosphate( $\text{PO}_4$ )	max	0.0003 %
Pyridine and homologues	max	0.001 %
sulphate ( $\text{SO}_4$ )	max	0.002 %

Table 7.2

Tartaric acid ( $C_4H_6O_6$ ) (G.R.)

B.N. OL801452

(Sarabhai M. Chemicals, Baroda, India)

Assay	min	99.5 %
In water insoluble substances	max	0.003 %
Residue on ignition (as $SO_4$ )	max	0.01 %
Arsenic (As)	max	0.00002 %
Calcium (Ca)	max	0.004 %
Chloride (Cl)	max	0.0005 %
Copper (Cu)	max	0.00005 %
Iron (Fe)	max	0.0003 %
Heavy metals (as Pb)	max	0.0003 %
Nickel (Ni)	max	0.0001 %
Oxalate ( $C_2O_4$ )	max	0.005 %
Phosphate ( $PO_4$ )	max	0.0005 %
Sulphate ( $SO_4$ )	max	0.005 %

is supported by the calculation of percentage deviation from the calculated<sup>d</sup> to observed value, given in Table 7.3. The deviations in some cases are positive and in other negative.

(d) Calculated percentage :

The chemical formula of d-AHT is  $\text{NH}_9\text{C}_4\text{O}_6$  ( $\text{NH}_4\text{H.C}_4\text{H}_4\text{O}_6$ ), having molecular weight 167.12<sup>2</sup> (Weast et al., 1964). From which percentage weight of each element in it is given in Table 7.3.

Table 7.3

Percentage of d-AHT elements				
Element	Calculated percentage	Observed percentage	Percentage deviation	
-----	<u>          </u> C	<u>          </u> O	<u>          </u> O-C	
1. C	28.75	29.31	+ 0.56	
2. H	5.43	5.06	- 0.37	
3. N	8.38	7.96	- 0.42	
4. O	57.44	57.68	+ 0.24	

The percentage difference, in the observed and calculated values of oxygen mentioned in the last column of the Table 7.3, namely + 0.24

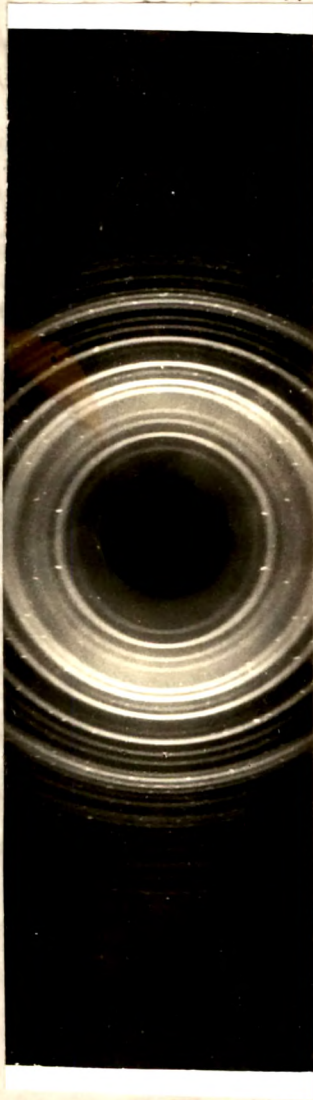
accounts for the experimental errors and the assay impurities present in the basic chemicals ammonium chloride, d-tartaric acid and sodium metasilicate. Looking to the availabilities of experimental techniques in the laboratory, it is difficult to ascertain the content of each impurity in the gel-grown crystals of d-AHT.

### 7.3 X-RAY DIFFRACTION METHOD

X-ray diffraction method is used to determine crystal structure of a material. In the present investigation, it is used to determine lattice parameters, ~~\_\_\_\_\_~~ and single crystalline character of d-AHT. The x-ray generator No. 1009, manufactured by M/s Phillips was employed. It was operated at 35 KV and 20 mA with a copper target and the *filtered/* unfiltered x-ray beam was used in the present work.

#### 7.3.1 Determination of lattice parameters

Debye-Scherrer powder method<sup>3</sup> (Azaroff and Buerger, 1958) of x-ray diffraction was employed to determine lattice parameters. *The filtered CuK radiation was used* Fig. 7.1 shows the powder pattern with the camera of radius  $R_p = 29.016$  mm.



X1.5

Fig. 7.1 X-ray powder photograph of d-AHT  
Camera radius is 29.016 mm

With an exposure of about 3 hrs, there was negligible intensity recorded in the back reflection region and hence only the front reflection region is shown in the figure. As can be seen in the pattern, there is quite a sufficient number of arcs available for measurement. However, at the same time the arcs are too closely spaced to allow accurate measurements. Therefore, the same pattern was obtained on a larger camera with radius  $R_F = 114.592$  mm giving quite sufficient separation of arcs. Due to the limited scanning range of this camera, many of the outer arcs were lost. Hence another camera of intermediate radius ( $R_F = 57.296$  mm) was also used to obtain the pattern. With such a combination of patterns, first eight arcs were measured on the film with  $R_F = 114.592$  mm and further six arcs were measured on the film with  $R_F = 57.296$  mm. The radii mentioned above are the actual radii of the cylindrical surfaces of films exposed to diffracted beams of x-rays.

The readings were made in succession on two corresponding arcs (left and right) by placing the indicator at the centre of each arc and recording the value with accuracy  $\pm 0.01$  cm. The sequence of separations can be best understood by preparing a data

sheet as shown in Table 7.4 . The larger reading is placed under the column heading  $x_2$  and the smaller under  $x_1$ . The difference of these two readings ( $S'$ ) gives diameter of arc. The next column contains the sum of  $x_1$  and  $x_2$ , which should remain constant with  $\pm 0.1$  mm accuracy. This is observed in the Table. Out of 14 lines (arcs), corrections are made for the first 8 arcs whereas readings for the remaining arcs except 13 are equal. Since the weightage of five observations for arcs 9-12 and 14 is much more than that for arc 13, it should have been rejected in usual analysis. However, for maintaining the sequence for arc 9-14, 0.05 mm is added to the reading for arc 13 so as to bring it in tune with other observations.

For correction P, mean of ( $x_2 + x_1$ ) is subtracted from each observation for line nos. 1 to 8. This correction is added in  $s'$  value. The Bragg angle  $\theta$  is calculated from corrected S value by the following equation :

$$\theta = \frac{S}{4R_p} \times \frac{180}{\pi} \quad (\text{in degrees}) \quad \dots(7.1)$$

T A U L S : 7.4  
 \*\*\*\*\*

Analysis of X-ray Powder Photograph  
 \*\*\*\*\*

Lines No : 1 to 8 taken from pattern by camera radius = R<sub>F</sub> = 114.592 mm

Lines No : 9 to 14 taken from pattern by camera radius = R<sub>F</sub> = 57.296 mm

$\sin^2 \theta_1 - \sin^2 \theta_n$ , where n = 1 to 13

Line No.	X1 (cm)	X2 (cm)	S' = X2-X1 (cm)	(X2+X1) S = 3 θ Sin <sup>2</sup> θ	Correc- tion = $\frac{X_2 - X_1}{X_2 + X_1} (S' - \delta)$	S (cm)	(cm)	1	2	3	4	5	6	7	8	9	10	11	12	13	
1.	4.69	10.25	5.56	14.94	0.008	5.568	6.96	0.0147													
2.	4.25	10.67	6.42	14.92	0.028	6.448	8.06	0.0197	0.0050												
3.	3.87	11.08	7.21	14.95	-0.002	7.208	9.01	0.0245	0.0098	0.0048											
4.	3.55	11.40	7.85	14.95	-0.002	7.843	9.81	0.0290	0.0143	0.0093	0.0045										
5.	2.89	12.06	9.17	14.95	-0.002	9.168	11.46	0.0395	0.0248	0.0198	0.0150	0.0105									
6.	2.63	12.31	9.68	14.94	0.008	9.688	12.11	0.0440	0.0293	0.0243	0.0195	0.0150	0.0045								
7.	2.35	12.60	10.25	14.95	-0.002	10.248	12.80	0.0491	0.0344	0.0294	0.0246	0.0201	0.0096	0.0051							
8.	2.10	12.84	10.74	14.95	0.008	10.748	13.43	0.0540	0.0393	0.0343	0.0295	0.0250	0.0145	0.0100	0.0049						
9.	4.57	10.40	5.83	14.97	0.00	5.83	14.56	0.0632	0.0485	0.0435	0.0387	0.0342	0.0237	0.0192	0.0141	0.0092					
10.	4.42	10.55	6.13	14.97	0.00	6.13	15.32	0.0698	0.0551	0.0501	0.0453	0.0408	0.0303	0.0258	0.0207	0.0158	0.0066				
11.	4.24	10.73	6.49	14.97	0.00	6.49	16.22	0.0780	0.0633	0.0583	0.0535	0.0490	0.0395	0.0340	0.0289	0.0240	0.0148	0.0082			
12.	4.10	10.87	6.77	14.97	0.00	6.77	16.92	0.0847	0.0700	0.0650	0.0602	0.0557	0.0452	0.0407	0.0356	0.0307	0.0215	0.0149	0.0067		
13.	3.8	11.12	7.32	14.92*	0.05	7.37	18.42	0.0998	0.0851	0.0801	0.0753	0.0708	0.0603	0.0558	0.0507	0.0458	0.0366	0.0300	0.0218	0.0151	
14.	3.47	11.50	8.03	14.97	0.00	8.03	20.07	0.1178	0.1031	0.0981	0.0933	0.0883	0.0783	0.0738	0.0637	0.0538	0.0446	0.0398	0.0331	0.0120	

-----

where  $S$  is arc in mm and

$R_F$  is radius of the camera used.

In the columns listed as 1,2,3 ..... n, the differences  $(\sin^2 \theta_1 - \sin^2 \theta_n)$  are calculated. The analysis of observations was carried out by Hesse-Lipson method<sup>3</sup> (Azaroff and Buerger, 1958) developed specially for orthorhombic system.

The interplanar spacing for the orthorhombic system can be written as :

$$\frac{1}{d_{hkl}} = \sqrt{\frac{h^2}{a^2} + \frac{k^2}{b^2} + \frac{l^2}{c^2}} \quad \dots (7.2)$$

On the other hand, the Bragg equation can be written in the form

$$\frac{1}{d_{hkl}} = \frac{2 \sin \theta_{hkl}}{\lambda} \quad \dots (7.3)$$

Equation (7.2) and (7.3) are squared and combined, to obtain the following relation ;

$$\frac{4 \sin^2 \theta_{hkl}}{\lambda^2} = \frac{1}{d_{hkl}^2}$$

$$= h^2 \frac{1}{a^2} + k^2 \frac{1}{b^2} + l^2 \frac{1}{c^2} \dots (7.4)$$

$$\begin{aligned} \text{or } \sin^2 \theta_{hkl} &= \frac{h^2 \lambda^2}{4 a^2} + \frac{k^2 \lambda^2}{4 b^2} \\ &+ \frac{l^2 \lambda^2}{4 c^2} \\ &= h^2 A + k^2 B + l^2 C \dots (7.5) \end{aligned}$$

$$\text{where } A = \frac{\lambda^2}{4a^2}, \quad B = \frac{\lambda^2}{4b^2}, \quad C = \frac{\lambda^2}{4c^2}$$

An interesting characteristic of equation (7.5) is that  $\sin^2 \theta$  is a simple sum of several parts, each part depending on its index h, k or l. Thus

$$\sin^2 \theta_{h00} = h^2 A \dots (7.6)$$

$$\& \sin^2 \theta_{0k0} = k^2 B \dots (7.7)$$

It follows that

$$\sin^2 \theta_{h00} + \sin^2 \theta_{0k0} = h^2 A + k^2 B \dots (7.8)$$

But this has exactly the same value as

$$\sin^2 \theta_{hko} = h^2 A + k^2 B \dots (7.9)$$

Consequently relationship of the following types occur :

$$\begin{aligned} \sin^2 \theta_{h_1 k_1 0} &= \sin^2 \theta_{h_1 0 0} + \sin^2 \theta_{0 k_1 0} \\ \sin^2 \theta_{h_1 k_1 l_1} &= \sin^2 \theta_{0 0 l_1} + \sin^2 \theta_{h_1 k_1 0} \\ \sin^2 \theta_{h_1 0 l_1} &= \sin^2 \theta_{h_1 0 0} + \sin^2 \theta_{0 0 l_1} \\ &\text{etc. } \dots (7.10) \end{aligned}$$

Difference relations also occur for example,

$$\begin{aligned} \sin^2 \theta_{0 k_1 0} &= \sin^2 \theta_{h_1 k_1 0} - \sin^2 \theta_{h_1 0 0} \\ \sin^2 \theta_{0 0 l_1} &= \sin^2 \theta_{h_1 k_1 l_1} - \sin^2 \theta_{h_1 k_1 0} \\ \sin^2 \theta_{0 0 l_1} &= \sin^2 \theta_{h_2 k_2 l_1} - \sin^2 \theta_{h_2 k_2 0} \\ &\text{etc. } \dots (7.11) \end{aligned}$$

The Hesse-Lipson method is based on the assumption that, if all possible combinations of  $\sin^2\theta$  values are used to form equations like those shown above, then the  $\sin^2\theta$  values in these equations are those of the pinacoid reflections (hoo), (oko), (00l).

By examining Table 7.4 the frequency of occurrence of various differences is tabulated below :

<u>Difference value</u>	<u>Occurrence</u>
0.0150	4 times
0.0049	3 times
0.0294	3 times
0.0343	3 times
0.0097	2 times
0.0200	2 times

Three values of  $\sin^2\theta_{100}$ ,  $\sin^2\theta_{010}$  and  $\sin^2\theta_{001}$  are selected according to equation 7.10 and 7.11. Two points are considered for selection. The first is to check whether higher order reflections

are present, that is, after  $\sin^2 \theta_{100}$  is selected, values of  $\sin^2 \theta_{200}$ ,  $\sin^2 \theta_{300}$  etc. should be observed in the table. The second point is that one or more of the  $\sin^2 \theta$  values of a pinacoid reflection must be equal to, or smaller than, the smallest value of the observed  $\sin^2 \theta$  values.

First of all, the smallest value is selected for  $\sin^2 \theta_{100}$ , which is equal to 0.0049 and which is observed three times. The higher order of which  $\sin^2 \theta_{200} = 0.0196$  is approximately equal to the value 0.0195 in the table. Even  $\sin^2 \theta_{300} = 0.0441$  which is nearer the value 0.0435. This means that the first selection is proper.

The second selection is made for  $\sin^2 \theta_{010}$  equal to 0.0097, occurring 2 times, the higher order of which is  $\sin^2 \theta_{020} = 0.0388$ . This approximately equals 0.0387, observed in the table.

The third value appears indirectly ; it can be calculated by taking  $\sin^2 \theta_{020} = 0.02$ , observed twice giving  $\sin^2 \theta_{010}$  equal to 0.010, which is present in the table. Other values are not useful because they do not satisfy the two conditions of equation 7.10 and 7.11.

For further verification, the above selected values are substituted into (7.10) and (7.11). The equations are found to be satisfied indicating selection to be proper. Now using following eqns, the three parameters are computed.

$$a^2 = \lambda^2/4 \sin^2_{100} \dots\dots (7.12)$$

$$b^2 = \lambda^2/4 \sin^2_{010} \dots\dots (7.13)$$

$$c^2 = \lambda^2/4 \sin^2_{001} \dots\dots (7.14)$$

where  $\lambda = 1.5418 \text{ \AA}^\circ$

By which  $a = 11.0129 \text{ \AA}^\circ$

$$b = 7.8273 \text{ \AA}^\circ$$

$$c = 7.7090 \text{ \AA}^\circ$$

These values are in reasonable agreement with those reported in the literature.<sup>4</sup> (Mullica, et al. 1979).

Thus the determination of lattice parameters also indicates that the crystal belongs to orthorhombic system.

### 7.3.2 Laue method :

The Laue method of x-rays is used to determine symmetry of d-AHT. In the present case, the same Phillips generator No. 1009 was used with copper target <sup>and unfiltered radiation</sup>. It was operated at 35KV and 20 mA. Unicam camera was used to take photographs.

An orthorhombic crystal has the following projection symmetries<sup>3</sup> (Azaroff and Buerger, 1958).

Direction	[100]	[010]	[001]	[0vw]	[uvw]
Symmetry	2 mm	2 mm	2 mm	m	1

This indicates that it has a 2-fold symmetry axis and two reflection planes perpendicular to all pinacoids. The photograph taken is <sup>with x-ray beam</sup> normal to cleavage plane, which implies 2-fold symmetry and two mirror lines (Fig. 7.2a). Because of crystal tilt, the Laue spots are not exactly at the corresponding symmetric positions. Fig. 7.2b shows the schematic diagram showing cleavage plane with respect to crystal habits (i) orthorhombic disphenoidal (ii) sphenoidal.

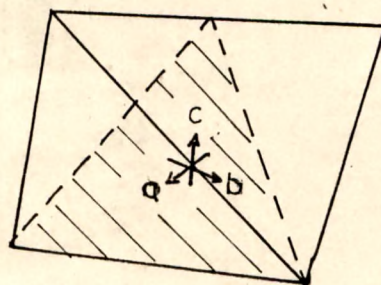
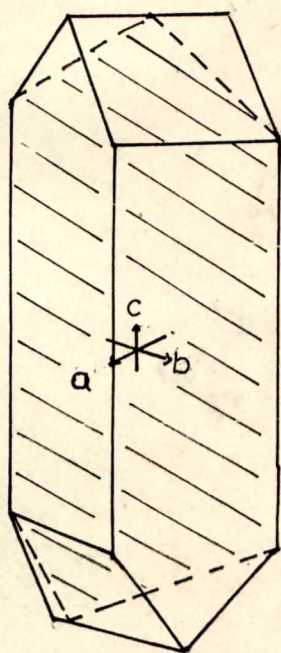
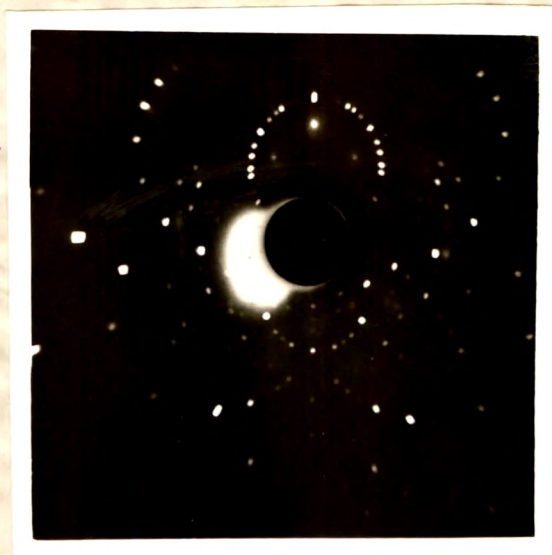


Fig. 7.2(a) Laue x-ray photograph of single synthetic d-AHT crystal, x-ray beam is normal to cleavage plane (010) of d-AHT.

Fig. 7.2(b) Schematic diagram of a cleavage plane shown by shaded region in  
 (i) orthorhombic disphenoidal and  
 (ii) sphenoidal d-AHT crystals.

It is thus, confirmed that the cleavage plane is one of the pinacoids. The indices are determined by stereographic projection. Besides the identification of plane, the Laue pattern also shows single crystallinity.

#### 7.4 INDICES OF THE GROWN FACES

The arrangement of habit planes on a crystal, when they are allowed to grow freely, follows the symmetry of the crystal and relative size developments follow successively increasing indices of plane. Moreover, the law of constancy of angles, a fundamental law of crystallography first observed by steno, extended by Domenico and later confirmed by Rome'de I' Isle<sup>5</sup> (Philips, 1971), served as a very useful tool for crystal identification. For orthorhombic crystal, all three parameters are different and the interaxial angles are each  $90^\circ$ . For ammonium-hydrogen-d-tartrate (d-AHT), the stereogram is prepared with the help of parameters and with its help, faces are indexed.

##### 7.4.1 Stereographic Projection of d-AHT

Stereographic projection is a versatile geometric

construction quite useful for crystallographic analysis<sup>of</sup> geometric data obtained from study of a crystal. It is also an attractive medium to represent crystallographic correlations of physical properties of a crystal. It is much used for determining crystal orientation, indexing surface markings such as slip lines, twins, deformation bands, cracks, etch pits, patterns made by magnetic powders, for solving crystallographic problems involved in precipitation, transformations in solid state and overgrowths.

In all the present study it has been used to index the habit faces of the grown crystals and in turn, to supplement the confirmation of the lattice system and lattice parameters inferred from x-ray powder diffraction data.

The stereographic projection is a projection of spherical space on a plane, the angular relations being preserved on the plane. In crystallography, it is projection of intersections of the normals to real or fictitious planes of a crystal infinitesimal in size and imagined to be positioned at the centre of the sphere. In principle, there are infinite

number of such planes defined for a crystal. However, in practice, only rational planes are useful since primarily only such planes significantly participate in the physical phenomena observable with a crystal.

If lattice parameters and interaxial angles for a crystal are known, the stereographic projection of the crystal can be prepared. Since, due to discreteness of distinct crystal structure, there are relations between the indices of a crystal plane being projected and the position of the corresponding projection. These result into the so-called zone-laws relating the plane-indices and indices of the zone to which a plane belongs. The mutual angular relations between various crystal planes represented by their indices are decided by the lattice parameters and the interaxial angles. For constructing the stereogram and analysing its data Wulff-net is a convenient graphical aid.<sup>6</sup> (Dana, 1985). The procedure of constructing stereogram of the d-APT crystal is described below. It is directly based on the correlation mentioned above and is applicable in general to any crystal once the lattice parameters and the interaxial angles of a crystal are known.

For the cubic system, stereographic projection is the same for all crystals because (i) all parameters are equal giving unit ratios and (ii) interaxial angles are constant ( $90^\circ$ ). For other systems, it varies from crystal to crystal. The stereogram displays symmetry of a system, as well as of a crystal in question.

Ammonium-hydrogen-d-tartrate (d-AHT) belongs to orthorhombic system, so all pinacoids are at  $90^\circ$ . The parameters are as follows :

(I) Reported by Mullica <sup>4</sup> (1979)	(II) Determined by author
a = 11.066 A <sup>o</sup>	11.013 A <sup>o</sup>
b = 7.843 A <sup>o</sup>	7.827 A <sup>o</sup>
c = 7.648 A <sup>o</sup>	7.709 A <sup>o</sup>

These can be normalized to the ratios taking largest value equal to unity i.e. 1.

(I) 1 : 0.7087 : 0.6911 (by reported values)	(II) 1 : 0.7107 : 0.7000 (by determined value)
---	---

To draw a stereogram of d-AHT, the Wulffnet is used. Plane of projection selected is (001), the

pole of which is plotted at the centre of the circle (Fig. 7.3). The other pinacoids are placed at  $90^\circ$  to each other along the circumference of the stereogram i.e. primitive circle.

To plot other poles, the following method is adopted. The angle between two vectors is defined by their dot product.

$$V_{h_1 k_1 l_1}^* \cdot V_{h_2 k_2 l_2}^* = r_1 r_2 \cos \theta \quad \dots (7.15)$$

where  $\theta$  = angle between vectors representing

$$(h_1 k_1 l_1) \text{ and } (h_2 k_2 l_2)$$

$$\begin{aligned} \cos \theta &= \frac{1}{V_1 V_2} V_{h_1 k_1 l_1}^* \cdot V_{h_2 k_2 l_2}^* \\ &= \frac{1}{V_1 V_2} (h_1 a^* + k_1 b^* + l_1 c^*) \cdot (h_2 a^* + k_2 b^* + l_2 c^*) \\ &= \frac{1}{V_1 V_2} h_1 h_2 a^{*2} + k_1 k_2 b^{*2} + l_1 l_2 c^{*2} \\ &\quad + (h_1 k_2 + k_1 h_2) a^* b^* \cos \psi^* \\ &\quad + (k_1 l_2 + l_1 k_2) b^* c^* \cos \alpha^* \\ &\quad + (l_1 h_2 + h_1 l_2) c^* a^* \cos \beta^* \\ &\dots (7.16) \end{aligned}$$



$$\cos \theta = d_1 d_2 \left[ \frac{h_1 h_2}{a^2} + \frac{k_1 k_2}{b^2} + \frac{l_1 l_2}{c^2} \right]$$

$$[\because \alpha = \beta = \gamma = 90^\circ \text{ and } \frac{1}{r_1} = d_1, \frac{1}{r_2} = d_2,$$

$$\frac{1}{a^*} = a, \frac{1}{b^*} = b, \frac{1}{c^*} = c$$

$$\text{But } |V_{hkl}^*| = \sqrt{V_{hkl}^* V_{hkl}^*}$$

$$\frac{1}{d_{hkl}} = \sqrt{(ha^* + kb^* + lc^*)(ha^* + kb^* + lc^*)}$$

$$= \sqrt{\frac{h^2}{a^2} + \frac{k^2}{b^2} + \frac{l^2}{c^2}}$$

$$d_{hkl} = \frac{1}{\sqrt{\frac{h^2}{a^2} + \frac{k^2}{b^2} + \frac{l^2}{c^2}}} \quad (\alpha = \beta = \gamma = 90^\circ)$$

substituting this <sup>in</sup> (7.16)

$$\cos \theta = \cos (h_1 k_1 l_1 \wedge h_2 k_2 l_2)$$

$$\frac{h_1 h_2}{a^2} + \frac{k_1 k_2}{b^2} + \frac{l_1 l_2}{c^2}$$

$$\therefore \cos \theta = \frac{\left( \frac{h_1^2}{a^2} + \frac{k_1^2}{b^2} + \frac{l_1^2}{c^2} \right) \left( \frac{h_2^2}{a^2} + \frac{k_2^2}{b^2} + \frac{l_2^2}{c^2} \right)}{\sqrt{\left( \frac{h_1^2}{a^2} + \frac{k_1^2}{b^2} + \frac{l_1^2}{c^2} \right) \left( \frac{h_2^2}{a^2} + \frac{k_2^2}{b^2} + \frac{l_2^2}{c^2} \right)}}$$

..... (7.17)

Using eqn. (7.17) the angles  $(111) \wedge (100)$  and  $(111) \wedge (001)$  are calculated and  $(111)$  is plotted at the calculated angles subtended by  $(111)$  with  $(100)$  and with  $(001)$ .

The angles between different faces were computed on the basis of parameters reported elsewhere and by the author and are presented in a tabular form.

Angle between faces	Angle calculated on the basis of		Difference B - A
	Reported parameters A	Parameters determined by author B	
$(111) \wedge (100)$	$63.67^\circ$	$63.49^\circ$	$- 0.16^\circ$
$(111) \wedge (001)$	$50.08^\circ$	$50.39^\circ$	$+ 0.31^\circ$
$(122) \wedge (001)$	$72.69^\circ$	$72.33^\circ$	$- 0.36^\circ$
$(212) \wedge (001)$	$85.00^\circ$	$84.77^\circ$	$- 0.23^\circ$
$(130) \wedge (100)$	$76.71^\circ$	$76.67^\circ$	$- 0.04^\circ$

In the same way, angles between other faces were also determined. It is clear from the above angles between corresponding faces that individually considered

the difference is quite noticeable. However, while plotting them on the Wulff's net and having a complete stereogram depicting different zones the difference loses its importance. This was checked by comparing two stereograms (one prepared from reported parameters and the other based on the parameters determined by the author). Hence, only one of them is retained and presented here.

With the help of the Wulff-net, the two zones defined by (111) with (100) and (111) with (001) are traced out. Where these two zones intersect, the (111) pole is plotted. In the same way, (121) and (211) poles are also plotted (Fig. 7,3).

For the plotted poles on a zone, zone law is used<sup>6</sup> (Dana, 1985). The zones defined by the pairs (100) & (001), (010) & (001) and (100) & (010) are drawn first. The first two are perpendicular diameters drawn from plotted pinacoids. The third is the primitive circle. As for example, indices of the pole occurring between  $(u\ v\ \omega)$  &  $(x\ y\ z)$  and on the zone defined by them will be  $(u + x, v + y, \omega + z)$ .

Also in the same way, the zone defined by (111) and (001) is drawn to intersect the primitive, the intersection being indexed as (110) on both sides. Same way, the zones defined by the pairs (010) & (111), (100) and (111), (010) and (121), (001) and (121), (001) and (211) etc. are drawn for further necessary poles. Thus with the help of zone law all intersections are indexed. Here on <sup>one</sup> the side, indices are shown without bar, to show the index on opposite side of axis, bar on the index number is used. Fig. 3 shows the stereogram of the d-AHT crystal.

#### 7.4.2 Miller indices for natural habit faces of d-AHT crystal :

Interfacial angles are measured by optical goniometer, described in Chapter-4. The d-AHT crystal is having one zone parallel to  $[001]$ . The crystal of the habit orthorhombic disphenoidal is used to find out zone angles. The crystal was stuck with plasticine on goniometer head such that the edge formed by the two faces was parallel to the goniometer axis. Keeping goniometer under table microscope and focusing all faces of the zone one by one, the observations were made having accuracy  $1'$ . In the

same way, the angles between sphenoidal faces were also measured.

Different zones and measured angles were checked for corresponding match on the stereogram. In the present case the primitive of the stereogram (Fig. 7.3) showing zone (010) and (100) is the major zone of the crystal. The ~~angles~~ faces are indexed according to matched poles. This is given in Table 7.5 and 7.6. Fig. 7.5a and 7.6a shows schematic diagram of crystals having different habits with symbols of faces. Other habits were indexed by similar comparison.

It is obvious from the comparison of calculated and observed values of interfacial angles that in some cases (marked with asterik in table 7.5) differences between their two values were noticeably large. There are several reasons for these differences. The orthorhombic disphenoidal crystal exhibits a large number of prism faces  $\{hko\}$ . The striations reported in Chapter-8, were prominent on these faces. These striations are parallel to the vertical edges of prism faces (i.e. C-axis). The whole model (cf. Fig. 8.5) was prepared on the basis of these observations (cf. Fig. 8.2 and 8.3). Further

the widths of the prism faces were rather very small and exhibit a large number of striations. As a result it is difficult to get consistent set of observations marked in Table 7.5. However, there were a few faces of larger widths for which consistency could be obtained. In addition to this, the (hko) faces were not flat. The faces with less widths were optically found to have noticeable curvature, which in turn affected marked observations significantly. As compared to these faces, the sphenoidal faces exhibit striations ; however the faces are having much bigger sizes. Hence on these faces plane areas, free from striations and curvature could be obtained. This produced fairly consistent results. Since experiments on chemical analysis, optical rotation and specific gravity of d-AHT<sup>15</sup> had invariably shown the material to ~~be~~<sup>is</sup> the d-AHT<sup>15</sup> for which the crystallographic data was available.<sup>2,4,7</sup> (Weast et al. 1964 ; Mullica et al. 1979 ; Vanbommel and Bijvoet ; 1958). Some adjustment while utilizing these observations in stereograms were made.

After careful consideration of the above factors, planes shown in Fig. 7.5a are indexed as follows :

<u>Reference plane</u>	<u>Designation index</u>	<u>Reference plane</u>	<u>Designation index</u>
1	(110)	I	(111)
2	(130)	II	( $\bar{1}\bar{1}\bar{1}$ )
3	( $\bar{1}\bar{1}$ 0)	III	( $\bar{1}\bar{1}\bar{1}$ )
4	( $\bar{1}$ 00)	IV	(1 $\bar{1}\bar{1}$ )
5	( $\bar{1}\bar{1}$ 0)	V	( $\bar{2}$ 13)
6	( $\bar{1}$ 30)	VI	(2 $\bar{1}\bar{2}$ )
7	( $\bar{1}\bar{1}$ 0)	VII	( $\bar{2}$ 13)
8	(100)	VII	(21 $\bar{2}$ )

In the orthorhombic disphenoidal habit, the sphenoidal faces are not plane, they are slightly curved, so the angles measured are approximately geometry-true angles. These faces are mixtures of different planes.

$$\begin{aligned}
 a &= (221), (111), (121) \\
 b &= (\bar{1}\bar{2}\bar{1}), (\bar{1}\bar{1}\bar{1}), (\bar{2}\bar{2}\bar{1}) \\
 c &= (\bar{1}2\bar{2}), (\bar{1}\bar{1}\bar{1}), (\bar{2}\bar{2}\bar{1}) \\
 d &= (2\bar{2}\bar{1}), (1\bar{1}\bar{1}), (1\bar{2}\bar{2})
 \end{aligned}$$

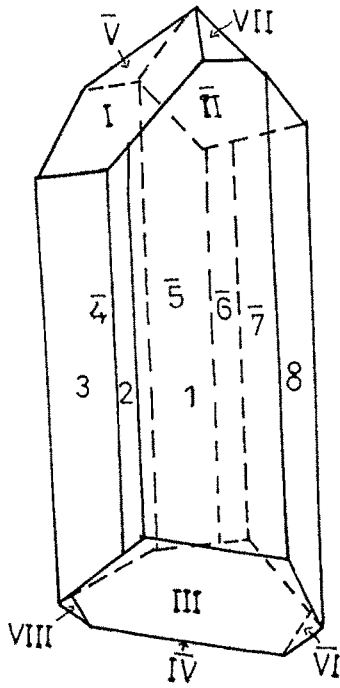


Fig. 7.5 (a) Sketch of orthorhombic disphenoidal crystal with symbols of faces.

(a)

Fig. 7.5 (b) Observed and calculated interfacial angles

Reference faces	Observed angle	Calculated angle
1 - 2	$25^{\circ} 9'$	$22^{\circ} 2'$
2 - 3	$43^{\circ} 51' 30''$	$48^{\circ} 37'$
3 - 4	$55^{\circ} 30'$	$54^{\circ} 40'$
4 - 5	$55^{\circ} 29' 30''$	$54^{\circ} 40'$
5 - 6	$25^{\circ} 45' 30''$	$22^{\circ} 2'$
6 - 7	$43^{\circ} 14' 30''$	$48^{\circ} 37'$
7 - 8	$55^{\circ} 30'$	$54^{\circ} 40'$
8 - 1	$55^{\circ} 30'$	$54^{\circ} 40'$

Fig. 7.5 (a,b) cont.

<u>Reference faces</u>	<u>Observed angle</u>	<u>Calculated angle</u>
I - 3	72° 50'	75° 17'
I - 2	45°	44° 41'
I - II	101°	100° 12'
II - 8	110° 46'	114° 15'
II - 7	73° 20'	75° 17'
VII - 1	113° 30'	117° 35'
VII - I	18° 22'	19° 44'
VII - II	35°	36° 49'
V - I	64° 4'	60° 46'
V - II	62° 30'	60° 40'
V - 5	90° 35'	89° 56'
III - 1	76°	75° 17'
III - 8	114° 25'	116° 20'
IV - 7	39° 53'	39° 55'
IV - 5	73° 10'	75° 17'
VIII - III	59° 12'	60° 44'
VIII - 4	56° 54'	58° 9'
VIII - IV	59° 33'	60° 36'
VI - III	87° 10'	88° 41'
VI - 7	50° 17'	52° 29'

These curved faces are observed when in a zone, more than four prismatic faces are observed. At the corners of sphenoidal faces, small faces are observed, having higher indices viz. (213) and (212).

The indices for reference faces given in Fig. 7.6a are as follows :

<u>Reference plane</u>	<u>Designation Index</u>
I	$(\bar{1}\bar{1}\bar{1})$
II	$(111)$
III	$(1\bar{1}\bar{1})$
IV	$(\bar{1}\bar{1}1)$

From observations of different crystal habits, it is found that four sphenoidal faces  $Z \{111\}$  are always present in the crystal habit, which are freely grown (except in needle-shaped crystals grown at the gel surface). Whereas in orthorhombic disphenoidal and needle-shaped crystals additionally four prismatic faces  $m(110)$  are always present. In zonal planes, (130) plane is always thinner than other planes, implying that it vanishes at a faster rate, and growth

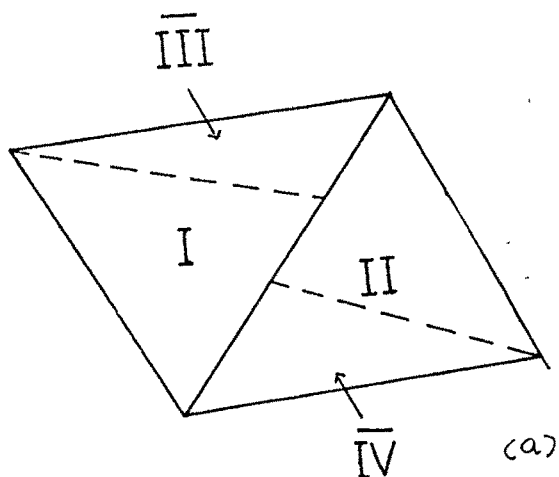


Fig. 7.6 (a) Sketch of sphenoidal crystal with symbols of faces

(b) Observed and calculated interfacial angles

(b)

<u>Reference faces</u>	<u>Observed angle</u>	<u>Calculated angle</u>
I - II	102°	100° 12'
I - III	101°	102° 31'
I - IV	129°	127° 20'
II - I	127°	127° 20'
II - IV	105°	102° 31'
III - IV	100°	100° 12'

rate is more in the direction normal to it. (100) plane is broader than other planes, which is perpendicular to cleavage plane. The corresponding axial parameter is also the biggest (11.0581 Å) that means in that direction the interatomic cohesion is the least and growth rate is also less.

The crystal belongs to space-group  $P_{2_1 2_1 2_1}$ . It has two fold symmetry about all the three axis and habits are also found to repeat according to the symmetry. About [100] direction crystal shows mirror images.

#### 7.5 SPECIFIC ROTATION

In case of liquids and solutions (which are organic compounds) optical activity is due to molecular structure. All substances, which show optical activity in liquid state or in solution have in their molecules some asymmetry. The molecules of optically active compounds possess at least one carbon atom joined to four different atoms or groups.

The substance (d-AHT) is dissolved in distilled water in different amounts (from 0.5 gm to 3.0 gm in

100 c.c. distilled water) and its optical rotation was measured by ARICO, polarimeter manufactured by Advance research instruments Co., made in India. The instrument is having least count 3' and monochromatic sodium light was used as source.

For zero reading, a tube having length of 2 decimeter was kept empty. After that, one by one solutions of different concentrations were filled in the tube. Care was taken that no air bubble remains in the path of light. The observations are recorded in Table 7.7. The graph is drawn for specific rotation  $\theta$  against mass  $m$  of d-AHT in 100 c.c. of distilled water (Fig. 7.4). The graph passes through origin. In all cases, rotation observed was dextro i.e. it rotates the plane of polarisation in a clockwise direction, when facing the source of light.

From graph, taking the slope  $\theta/m$  and substituting it in following equation.

$$\text{Specific rotation} = \frac{100 \times \theta}{lm} \quad \dots (7.18)$$

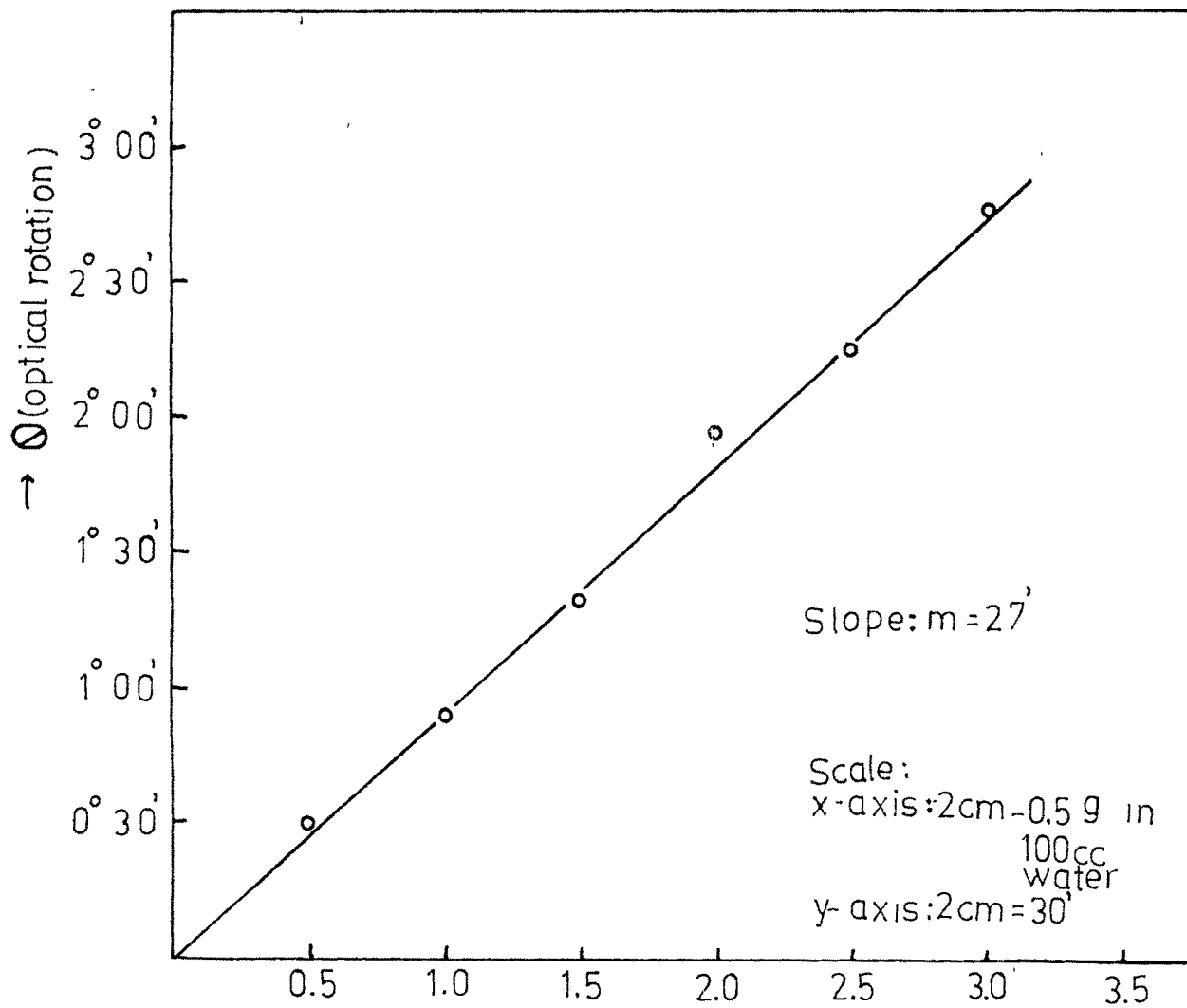
Table 7.7

Readings of optical rotation for different concentrations of d-AHT aqueous solution

---

m gram in 100 c.c. of distilled water (in gm)	Polarimeter observation (in degree)		Observed rotation	
zero reading	0°	0'	-	
0.5	0°	30'	0°	30'
1.0	0°	55'	0°	55'
1.5	1°	22'	1°	20'
2.0	1°	57'	1°	57'
2.5	2°	15'	2°	15'
3.0	2°	46'	2°	46'

---



→ C gm in 100cc water

Fig. 7.4

where  $\theta$  = observed angle

$l$  = length of the tube (in decimeter)

$m$  = gram of optically active substance in  
100 c.c. of distilled water

can be determined

$$s = \frac{100 \times 0.45}{0.5 \times 2} \quad (\text{here } 27' \text{ from graph is converted into decimal})$$

Specific rotation  $S = +45$  (\* sign due to clockwise rotation)

The rotation of the solution is found dextro which may be due to the fact that one of the reactants used to grow crystal is dextro rotatory tartaric acid. This is supported by the data in the literature.

#### 7.6 SPECIFIC GRAVITY OF CRYSTAL

The specific gravity (S.G.) of d-AHT was determined by specific gravity bottle. The specific gravity is defined as : the weight of the body divided by the weight of an equal volume of water. The crystal is partially soluble in water, whereas it is insoluble in

which  
kerosene<sub>x</sub> was used to determine S.G. of d-AHT crystal.

The observations and calculations are as under :

- (i) Wt. of empty specific gravity bottle =  $W_1 = 19.504$  gm
- (ii) Wt. of S.G. bottle + Crystals =  $W_2 = 20.430$  gm
- (iii) Wt. of S.G. bottle + crystals + Kerosene =  $W_3 = 60.129$  gm
- (iv) Wt. of S.G. bottle + kerosene =  $W_4 = 59.660$  gm at  $23^\circ\text{C}$
- (v) Wt. of S.G. bottle + dist. water =  $W_5 = 69.375$  gm at  $23^\circ\text{C}$

$$\begin{aligned} \text{Sp gr of kerosene} &= \rho' = \frac{W_4 - W_1}{W_5 - W_1} \\ &= \frac{40.156}{49.871} \\ &= 0.805 \end{aligned}$$

$$\begin{aligned}
 \text{S.G. of d-AHT crystal} &= \frac{W_2 - W_1}{[(W_4 - W_1) - (W_3 - W_2)]} \times S' \\
 &= \frac{0.926}{40.156 - 39.699} \times 0.805 \\
 &= \frac{0.836}{0.457} \times 0.805 \\
 &= 1.631
 \end{aligned}$$

Several determinations of S.G. were made. The mean value of  $\rho_{sp}$  is  $1.631 \pm 0.002$ .

Dislocation density on a cleavage plane is determined by etch technique (cf. Chapter-8) Knoop hardness number & Vickers hardness number under an applied load,  $35.4 \text{ kg/mm}^2$  and  $51.2 \text{ kg/mm}^2$  are determined by employing Knoop and Vickers indenters (cf. Chapter-11). Table 7.8 summarizes all characterizations made by the author.

Table 7.8

Characteristics of synthetic d-AHT crystals grown  
in silica gel

Sr. No.	Property studied	
1.	Crystal habits and Maximum size obtained	
	(a) needle shaped	42 x 11 x 11 mm
	(b) orthorhombic disphenoidal	21 x 9 x 6 mm
	(c) sphenoidal	10 x 10 x 8 mm
2.	Colour	Colourless
3.	Taste	Savour
4.	Faces obtained	{100}, {110}, {130} {111}, {213}, {212}
5.	Unit cell dimensions	a = 11.013A <sup>o</sup> b = 7.827A <sup>o</sup> c = 7.709A <sup>o</sup>
6.	Density	1.631 gm cm <sup>-3</sup>
7.	Average microhardness at R.T. 30 <sup>o</sup> C	
	(a) Knoop hardness	35.4 kg mm <sup>-2</sup>
	(b) Vickers hardness	51.2 kg mm <sup>-2</sup>
8.	Estimated dislocation density	5 x 10 <sup>5</sup> cm <sup>-2</sup>
9.	Decomposition temperature at atmospheric pressure	120 <sup>o</sup> C
10.	Optical rotation of aqueous -d-AHT	+45

## REFERENCES

1. HENDRICKSON, J.B. ; 1970 Organic Chemistry,  
CRAM, D.J. and 3rd ed, McGraw-Hill,  
HAMMOND, G.S. Kogakusha Ltd.,  
Tokyo
  
2. WEAST, R.C. ; 1964 Handbook of Chemistry  
SELBY, S.M. and and Physics, 45th  
HODGMAN, C.D. ed., The chemical  
Rubber Co., Ohio,  
pp B-152
  
3. AZAROFF, L.V. and 1958 The powder method  
BUERGER, M.J. in x-ray crystallo-  
graphy, McGraw-Hill  
book Co. Inc., N.Y.  
p. 83.
  
4. MULLICA, D.F. ; 1979 J. Appl. Cryst.,  
BEALL, G.W. ; 12, 263  
MILLIGAN, W.O. and  
OLIVER, J.D.
  
5. PHILLIPS, F.C. 1971 An Introduction to  
Crystallography.  
ELBS.
  
6. DANA, F.S. 1985 A Textbook of minera-  
logy, Asia Publishing  
House, Bombay IV ed.  
p. 61
  
7. VANBOMMIL, A.J. and 1958 Acta. Cryst. 11,  
BIJVOET, J.M. 61.

List of Tables :

- 7.1 Assay of Ammonium chloride given by manufacturer,  
Sarabhai M. Chemicals, Baroda, India
- 7.2 Assay of d-Tartaric acid given by manufacturer,  
Sarabhai M. Chemicals, Baroda, India
- 7.3 Percentage of d-AHT elements
- 7.4 Analysis of X-ray powder photograph
- 7.5 (a) Sketch of orthorhombic disphenoidal crystal  
with symbols of faces
- (b) Observed and calculated interfacial angles
- 7.6 (a) Sketch of sphenoidal crystal with symbols  
of faces.
- (b) Observed and calculated interfacial angles.
- 7.7 Readings of optical rotation for different  
concentrations of d-AHT aqueous solution.
- 7.8 Characteristics of synthetic d-AHT crystals  
grown in silica gel.

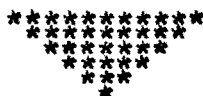
CAPTIONS TO THE FIGURES

- 7.1 X-ray powder photograph of d-AHT. Camera radius is 29.016 mm.
- 7.2 (a) Laue x-ray photograph of single synthetic d-AHT crystal. X-ray beam is normal to cleavage plane (010) of d-AHT.
- (b) Schematic diagram of a cleavage plane shown by shaded region in (i) orthorhombic disphenoidal and (ii) sphenoidal d-AHT crystals.
- 7.3 General stereogram of d-AHT crystal.
- 7.4 Plot of optical rotation of d-AHT with concentration of aqueous solution of d-AHT.

CHAPTER - 8

CHEMICAL DISSOLUTION OF  
d-AHT CLEAVAGES

	<u>PAGE</u>
8.1 Introduction   ... ..	160
8.2 Experimental   ... ..	161
8.3 Observations and discussion   ... ..	162
8.4 Conclusions   ... ..	171
References	



## 8.1 INTRODUCTION

Dissolution of a crystal surface occurs by retreat of monomolecular steps, being reverse to that of growth, which takes place due to motion of steps on a surface. The microtopographical study of grown faces of a crystal provides information about mechanism of growth, whereas dissolution reveals early stages of growth and/or defect structure. Several investigators had carried out microtopographical study of natural grown faces and/or theoretical work to unfold growth mechanism (e.g. Verma, 1951<sup>1</sup> ; Augustine and Hale, 1960<sup>2</sup> ; Desai, 1979<sup>3</sup> ; Joshi et al. 1980<sup>4</sup> ; Frank, 1949<sup>5</sup> etc.) Since the classic work on controlled chemical dissolution of LiF crystals was made by Gilman (1958) and his collaborate,<sup>6</sup> much work in this direction has appeared in the literature on dissolution e.g. see Ives and Mcausland (1963),<sup>7</sup> Ives and Hirth (1960)<sup>8</sup>, Urusovkaya (1965)<sup>9</sup>, Haribabu and Bansigir (1969)<sup>10</sup>, Raju Bhagwan et al. (1970)<sup>11</sup>, Raju and Bhagwan (1971)<sup>12</sup>, Sangwal and Patel (1978)<sup>13</sup>, Popkova and Predvoditelev (1970)<sup>14</sup>, Popkova et al. (1969)<sup>15</sup>, Pandya and Tolansky (1954)<sup>16</sup>, Ram et al. (1973)<sup>17</sup>, Takoo (1985)<sup>18</sup>, Bhagia and Pandya (1985)<sup>19</sup>, Shah and Pandya (1985)<sup>20</sup> etc. As a part of programme of studying dissolution phenomena on crystal surfaces

e.g. see Mehta (1972)<sup>21</sup>, Acharya (1978)<sup>22</sup>, Shah (1976)<sup>23</sup>, Bhagia (1983)<sup>24</sup> and Shah (1984)<sup>25</sup>, the present work on controlled chemical dissolution of synthetic single crystals of d-AHT is taken up and reported here. The primary aim is to determine qualitatively density of dislocations of the grown crystals.

## 8.2 EXPERIMENTAL

Chemical dissolution of natural faces and cleavage faces of synthetic d-AHT crystals of different habits grown in a silica gel medium was optically studied. There are several habits exhibited by synthetic d-AHT crystals; they are shown in figure 8.1<sup>(b)</sup> along with their line diagrams. Since d-AHT is slightly soluble in water (3.2 gm in 100 cc of water), the natural faces were cleaned by well-known liquid cleaners and/or rinsers free from water, such as petroleum ether, Xylene, absolute alcohol etc. The cleavage faces were produced in the usual way. By trial and error method, it was found that water, formic acid, a solution of crystalline trichloroacetic acid in a fixed amount of glacial acetic acid were suitable for delineating defect structure on crystal faces. The etching was

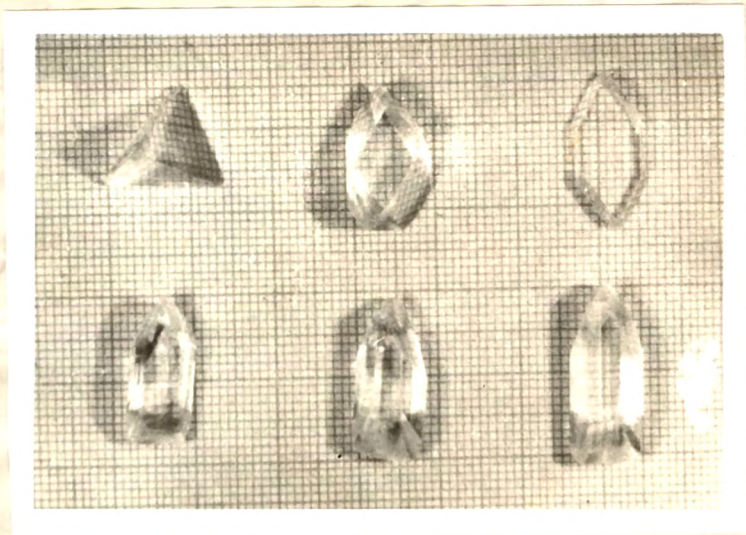
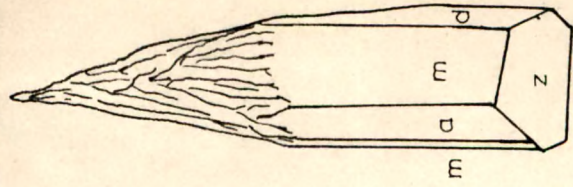
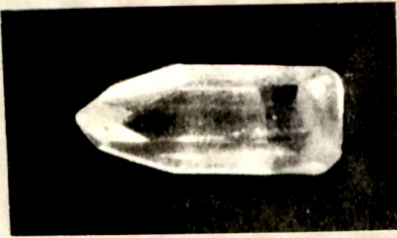
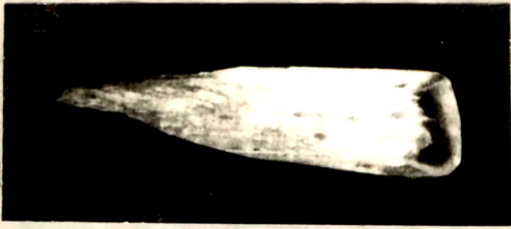
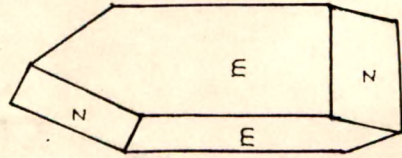


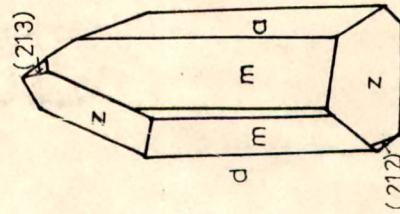
Fig. 8.1(A) A Comparative sizes of various crystal habits of d-AHT



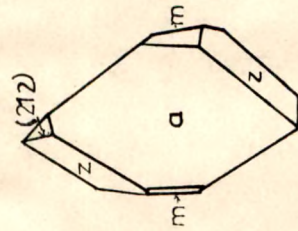
(f)



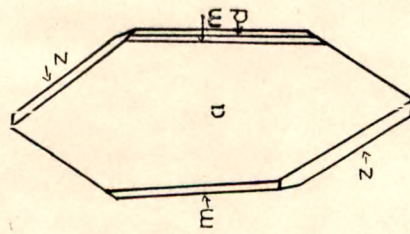
(e)



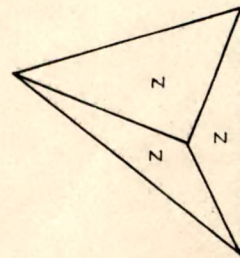
(d)



(c)



(b)



(a)

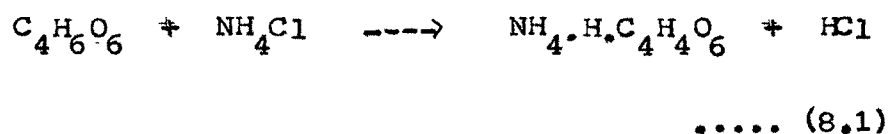
z (111)  
 m (110)  
 a (100)  
 d (130)

Fig. 8.1(b)

carried out by dipping a crystal in an etchant for a fixed time in static condition of etchant at room temperature (30°C). The etched samples were rinsed by alcohol and dried by hot air blower. The C-Z VERTICAL microscope, described in Chapter-2, was employed to carry out microtopographical study of the natural and cleavage faces of d-AHT.

### 8.3 OBSERVATIONS AND DISCUSSION

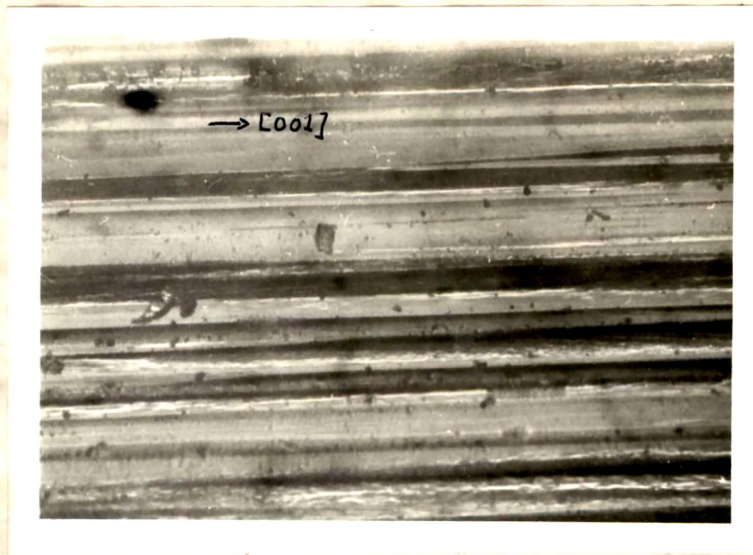
From a study of a large number of sphenoidal and orthorhombic faces, it was noticed that a large number of growth features were intimately mixed with etch features, due to the fact that in a chemical reaction between d-tartaric acid impregnated gel and ammonium chloride solution (FS)



along with the formation of d-AHT nuclei, hydrochloric acid nuclei were also formed. Further water was already available in the gel and FS. d-AHT is soluble not only in water but it also reacts with HCl. As a result the growth and chemical dissolution of d-AHT

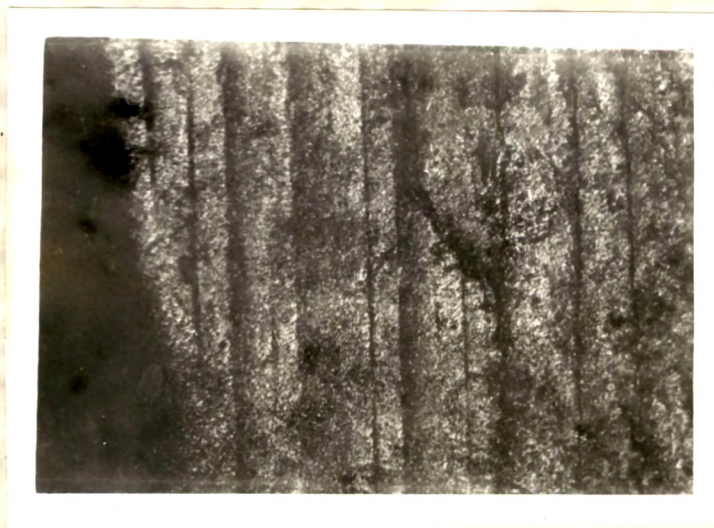
occur simultaneously. Since the growth process is more dominant of the two, the faces do grow. It is not possible to detect accurately when the growth process is completed and the chemical dissolution has an edge over the former. The result is the mixture of growth and dissolution patterns on the natural faces. It is obviously difficult to separate the two features in a conclusive manner. However, of all the features, one feature which was consistently observed on the prism faces  $\{hKO\}$  has striations, consisting of a series of parallel lines running over the entire face. Same were also observed on a cleavage face, etched by hydrochloric acid. The etching was so fast that even in 2-3 seconds deeply etched striations were observed. Hence this etchant was not used for delineating dislocations on a cleavage surface. Further it can be conjectured from this action of hydrochloric acid on  $d-AHF$  cleavages that the striations and layered structures observed on natural prism and sphenoidal faces are most likely to be due to etching of these faces by hydrochloric acid produced from the chemical reaction between ammonium chloride and TA impregnated SMS. This etching action produces ' growth striations ' of unequal depths

and elevations and also their non-uniform spacing. At the same time, this suggests that in the growth of d-AHT, striations play an important role. These striations have  $[001]$  direction, the direction of crystal growth axis of d-AHT. Figure 8.2 is a photomicrograph of striations on a prism face  $(110)$ . It shows that striations are parallel to C-axis and depressions of varying depths. The spaces between consecutive striations is not constant. Further some are shallow and some are deep. On a large number of sphenoidal faces  $\{111\}$ , a layered structure similar to that of figure 8.2 was observed. Fig. 8.3 represents such a layered structure starting from a sphenoidal edge and ending on the other. It is now well-known from the theory of crystal growth that corners and edges can serve as the initiation sites for growth layers. The distinguishing feature of these layers as compared to those observed in Fig. 8.2 is that many of them are quite sharp. Water and unsaturated solution of d-AHT in water (3.2 gm d-AHT in 100 c.c. of water form a saturated solution at  $25^{\circ}\text{C}$ ) can also act as etchants. Controlled etching of prism and cleavage faces by one of the above etchants produced needle shaped etch pits<sup>of</sup> assorted sizes parallel to direction  $[001]$  (Fig. 8.4). This also suggests that striations are associated in some



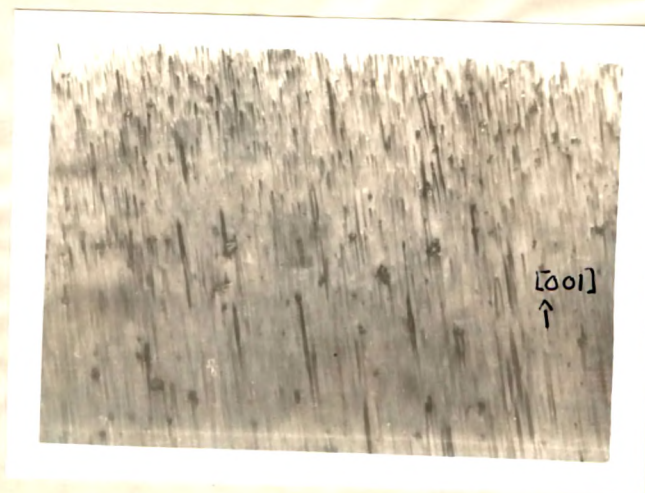
x 25

Fig. 8.2 Striations on a prism face (110) parallel to  $[001]$



x 25

Fig. 8.3 Layered structure on a sphenoidal face (111) with lines parallel to each other and starting from a sphenoidal edge and ending on the others

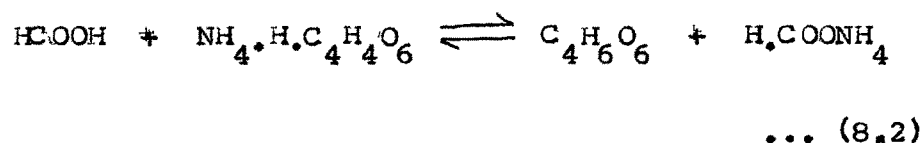


x 200

Fig. 8.4 Needle-shaped etch pits of assorted sizes produced by etching d-ATP prism face (110) by distilled water for two seconds

way with the growth of d-AHT crystals. From a detailed study of such patterns on a large number of prism and sphenoidal faces and also from the earlier study of habit faces of d-AHT, it is possible to conjecture the growth of a full fledged orthorhombic disphenoidal crystal. The cluster of needles with their cross sectional edges arranged in a particular manner can create orthorhombic disphenoidal crystal (Fig. 8.5). The growth of different prism faces would obviously change the cross-sectional sphenoidal edges.

Formic acid (98%) was also used as an etchant for d-AHT crystals. The chemical reaction and dissolution between formic acid and d-AHT is very rapid. It is given by



The reaction is reversible. The reaction produces comparatively large etch pits within a few seconds. Fig. 8.6 is a typical photomicrograph of etch pits produced on a fresh cleavage surface of d-AHT. It shows a big point bottomed pit with trapezium as a

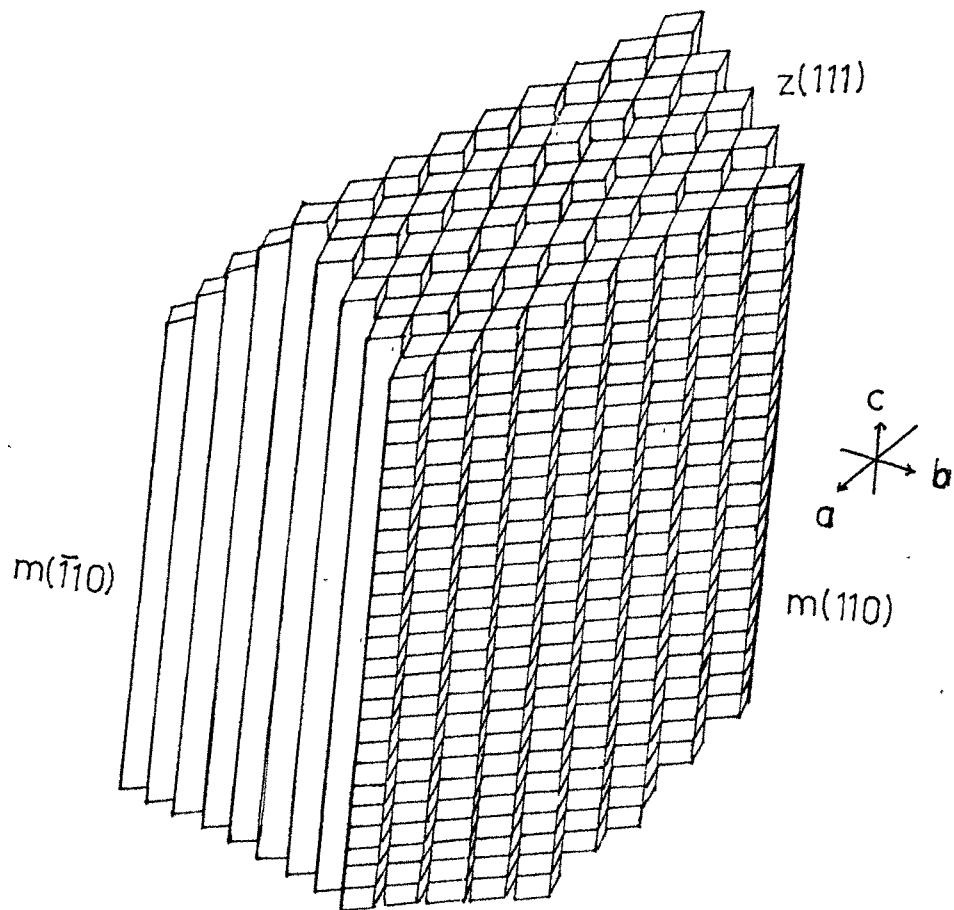


Fig. 85

plane outline on observational surface and micropitting over the entire surface. The parallel sides of the trapezoidal etch pits are parallel to C-axis and the longer diagonal of the trapezium makes an angle of  $45^{\circ}$  with C-axis (along  $[101]$ ). Further one side of the etch pit is curvilinear (Fig. 8.6) indicating that the basic etch pit for a certain etchant concentration should be a pentagonal etch pit which could be point-bottomed or flat-bottomed. Fig. 8.6 also exhibits a large number of grooves parallel to each other and to the etch pit sides. The formation of etch pits in these grooves indicates that etch pits are produced at the sites of a specific type of defects, likely to be of a class of linear defects. It is clear from the shape of a pit that the depth point does not coincide with the geometric centre of the pit, giving rise to eccentricity. It was found that almost all pits observed on the cleavage surface were eccentric. The eccentricity changes with concentration. This supports the observations on the eccentricity of etch pits, studied on a cleavage surface of calcite, etched by organic and inorganic acids under different conditions.<sup>26-31</sup> (Mehta and Pandya, 1982 ; Mehta, 1980 ; Mehta, 1981 ; Pandya and Mehta, 1969 ; Pandya

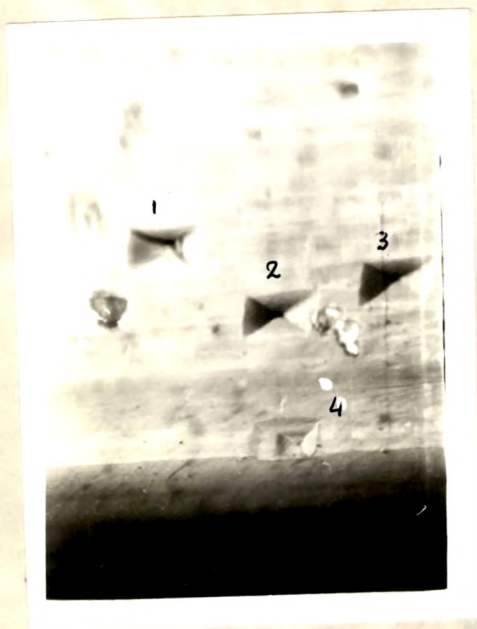
and Bhagia, 1983). The matching of etch patterns on the oppositely matched cleavage counterparts was also studied. Fig. 8.7a,b represent cleavage counterparts of d-AHP etched by concentrated formic acid (98%) at room temperature, for 5 seconds. There is a one to one correspondence between the shape, orientation and location of etch pits, which are numbered for the sake of convenience. Further, the sizes of etch pits on one photomicrographs are little different from those on the other. This is due to the fact that etching time is very small and that a little change in rinsing process of etched crystals enhances further etching of cleavage plane of d-AHP. The striations are also etched, giving rise to series of faint lines parallel to each other having direction  $[001]$ . Further, depths and elevations of striations are different, hence striations which formed deep grooves are etched faster, giving rise to thick dark lines, similar to strips. These matching of pits indicates that they reveal dislocations intersecting the observational plane.

Crystalline trichloroacetic acid dissolved in glacial acetic acid produces an etchant mixture, which is capable of creating etch pits. Further the plane

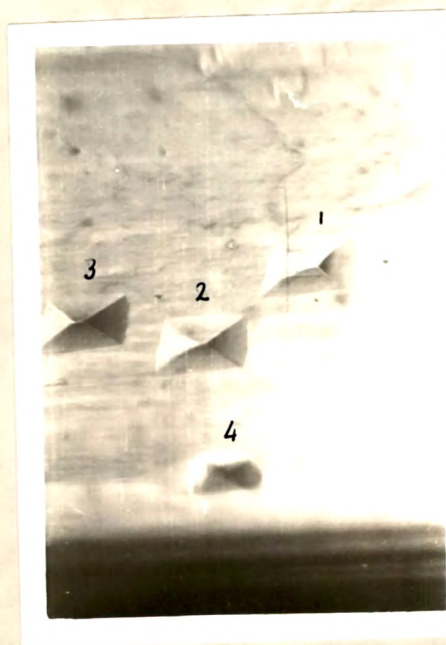


x250

Fig. 8.6 Trapezoidal etch pit on a cleavage plane (010) produced by formic acid (etching time 5 sec. at 30°C) parallel sides are having direction 001



(a)



(b)

x125

Fig. 8.7a,b Matching of cleavage counter parts etched by formic acid for 5 sec. showing one-to-one correspondence between etch pits.

shape of etch pits on a cleavage surface is dependent on the amount of crystalline trichloroacetic acid in a fixed amount of glacial acetic acid. Fig. 8.8a,b represent oppositely matched cleavage counterparts etched by a solution of 5 gm of trichloroacetic acid in 100 c.c. of glacial acetic acid for a minute at room temperature. An excellent correspondence between the location, size and shape of etch pits on cleavage counterparts is noticeable. This also indicates that the etch pits are at dislocations ending on a cleavage surface. The density of etch pits produced by formic acid and also by a solution of trichloroacetic acid in glacial acetic acid is  $\sim 5 \times 10^5/\text{cm}^2$ . This represents the average of the density values calculated from a large number of matched surfaces (about 2 dozens).

The variations of quantity of crystalline trichloroacetic acid in a fixed quantity of glacial acetic acid changes the pit shapes on a cleavage surface of d-AHT. Fig. 8.9 is a photomicrograph of cleavage surface etched for 60 seconds by an etchant containing 5 gm of trichloroacetic acid in 100 c.c. of glacial acetic acid, at room temperature (30°C). The etch pattern consists of curvilinear trapezoidal



x 200

(a)

(b)

Fig. 8.8a,b Matching of cleavage counter parts etched by mixture of 5 gm trichloroacetic acid in 100 c.c. glacial acetic acid for 60 sec.

etch pits. The parallel sides and longer diagonal make angles of  $60^\circ$  and  $45^\circ$  respectively with C-axis i.e. direction  $[001]$ . They are directed along  $[201]$  and  $[101]$  respectively. The shorter diagonal is normal to C-axis, whereas striations on the surface are parallel to C-axis.

Fig. 8.10 represents elongated triangular etch pits pointing in the direction  $[201]$  and produced by etching in a solution of 10 gm of trichloroacetic acid in 100 c.c. of glacial acetic acid for 90 sec. It also exhibits shallow vertical striation in the direction  $[001]$ . Assorted elliptical pits (Fig. 8.11) with major axis in the direction  $[201]$  are produced by etching a cleavage surface in a solution of 15 gm of trichloroacetic acid in 100 c.c. of glacial acetic acid for a period of 120 sec. It should be noted that on the left hand side of this photomicrograph is a heavily etched striation showing the formation of etch pits along it. In this part, the unevenness of the etched surface is quite noticeable. Leaf-shaped etch pits of varying sizes (Fig. 8.12) in the direction  $[201]$  are observed, when d-AHF cleavage surface was etched by solution containing 20 gm of trichloroacetic acid in 100 c.c. glacial

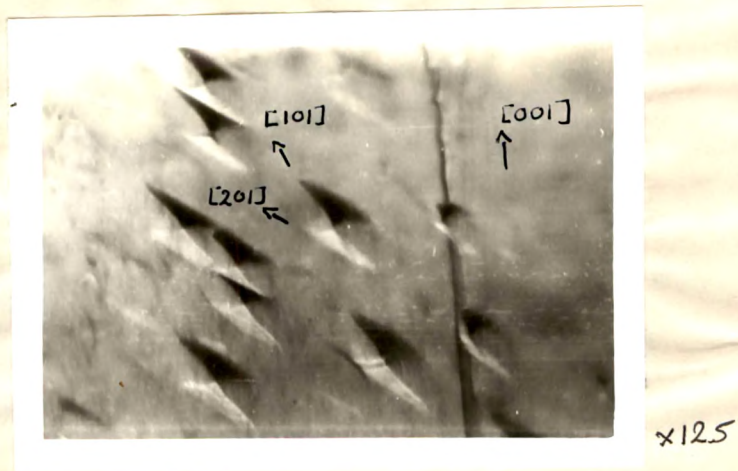


Fig. 8.9 Curvilinear trapezoidal etch pits on cleavage plane, by solution of 5 gm trichloroacetic acid in 100 cc of glacial acetic acid for 60 sec. at 30°C.



Fig. 8.10 Triangular etch pits on cleavage plane, obtained by etchant 10 gm trichloroacetic acid in 100 c.c. glacial acetic acid for 90 sec. at 30°C.

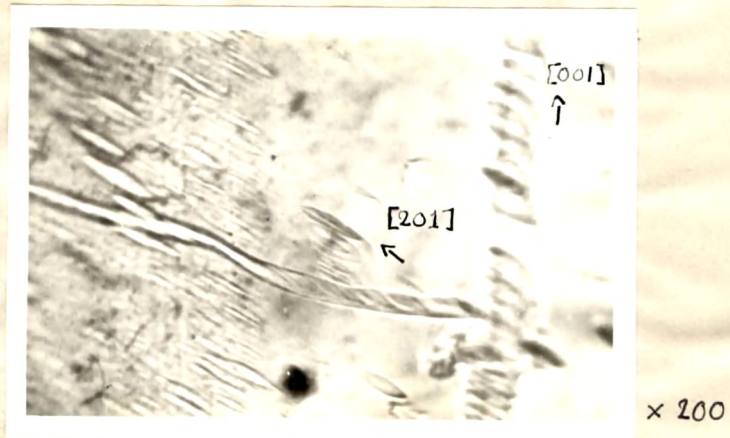


Fig. 8.11 Elliptical-shape etch pits on cleavage surface by 15 g. trichloroacetic acid in 100 cc. glacial acetic acid for 120 sec. at  $30^{\circ}\text{C}$

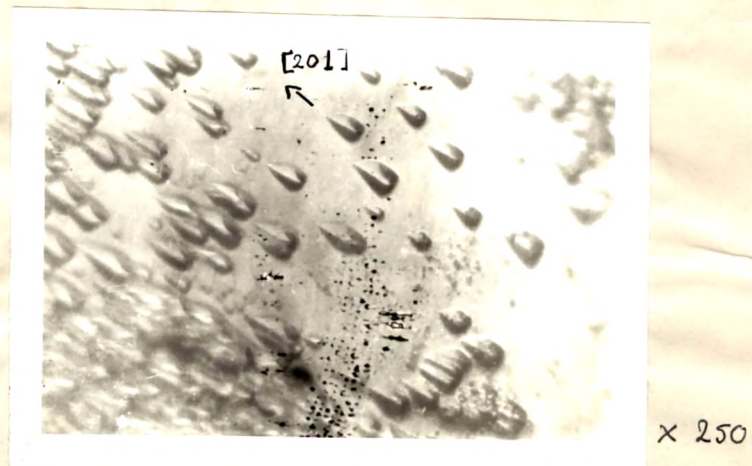


Fig. 8.12 Leaf-shaped etch pits on cleavage surface by 20 gm trichloroacetic acid in 100 c.c. glacial acetic acid for 180 sec. at  $30^{\circ}\text{C}$

acetic acid for 180 sec. It is thus clear that as the amount of trichloroacetic acid in 100 c.c. of glacial acetic acid is progressively increased from 5 gm to 20 gm, the plane outline of an etch pit changes from a curved trapezium to elongated triangle, to ellipse and finally to a leaf-like shape. They are schematically represented in the Table 8.1. This type of changes in the plane shape of etch pits was also observed while studying chemical and thermal dissolution of calcite cleavages by varying concentrations of organic and inorganic acids<sup>26-31</sup> (Mehta and Pandya, 1982 ; Mehta, 1980 ; Mehta, 1981 ; Mehta, 1981 ; Pandya and Mehta, 1969 ; Pandya and Bhagia, 1983) at room temperature and thermal<sup>21,23-25</sup> dissolution of calcite cleavages at high temperatures. (Mehta, 1972 ; Shah, 1976 ; Bhagia, 1983 ; Shah, 1984). Similar explanations based on anisotropic etch rates and eccentricity can be given for these changes in plane-shape.

It was reported above that d-AHT cleavage surface etched by a solution of 15 gm trichloroacetic acid in 100 c.c. glacial acetic acid at 30°C exhibits elliptical pits (Fig. 8.11). The multiple etching of a cleavage surface by the above solution for 45, 90,

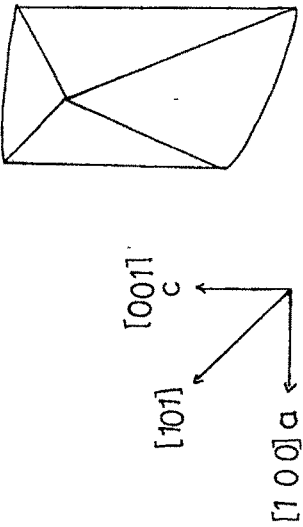
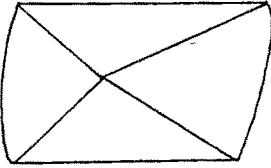
Table 8.1

Shape-cycle of etch pits produced by varying quantity of crystalline trichloroacetic acid in 100 c.c. of glacial acetic acid at 30°C on a cleavage surface of d-AT.

<u>Etchant</u>	<u>Schematic diagram</u>	<u>Remarks</u>
1. 100 c.c. glacial acetic acid + 50 trichloroacetic acid		Curvilinear trapezoidal shaped etch pit, having two parallel sides along $[20]$ longer diagonal along $[10]$
2. 100 c.c. glacial acetic acid + 10 g trichloroacetic acid		Triangular shaped etch pits, making 60° to C-axis i.e. along $[20]$ direction.
3. 100 c.c. glacial acetic acid + 15 g trichloroacetic acid		Elliptical shaped etch pit along $[20]$ direction
4. 100 c.c. glacial acetic acid + 20 g trichloroacetic acid		Leaf-like shape/etch pit, along $[20]$ direction

Table 8.2

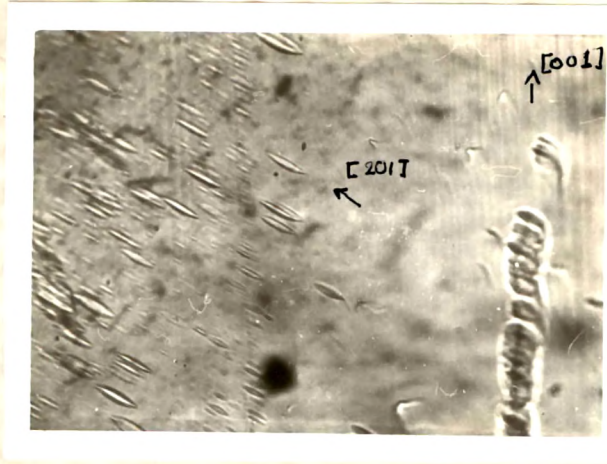
Schematic diagram of etch pits produced by formic acid at 30°C, on a cleavage surface of d-AHT

<u>Etchant</u>	<u>Schematic diagram</u>	<u>Remarks</u>
1. Formic acid		<p>Trapezoidal etch pits, having two parallel sides, parallel to crystallographic C-axis and longer diagonal inclined at an angle of 45° with C-axis</p>
2. Formic acid		<p>Trapezoidal etch pits, having two parallel sides, parallel to crystallographic C-axis and longer diagonal inclined at an angle of 45° with C-axis</p>

135 and 170 seconds, is shown in Fig. 13(a,b,c,d). It is noticeable that pit shape remains unchanged, however their sizes increase with etching time and as a result they begin to coalesce, the pit density practically remains unchanged. The etching of a striation produces a series of etch pits along it. The successive etching for this point of the surface is faster than the rest of the surface and as a result it is slightly out of focus as compared to the rest of the etched surface under observation. Tables 8.1 and 8.2 present brief features of etching by the etchants used to produce selective etching d-AHT cleavages.

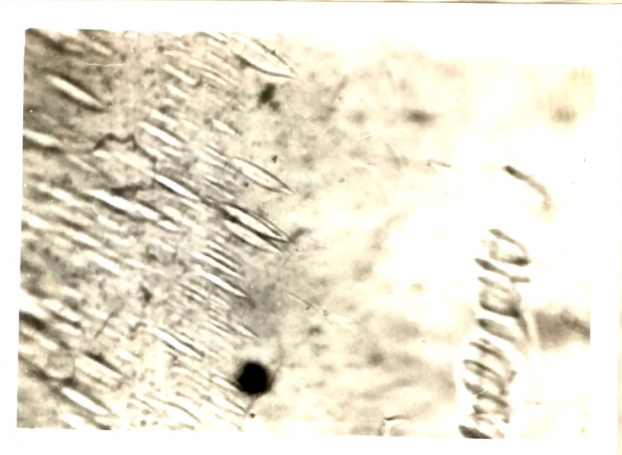
#### 8.4 CONCLUSIONS

- (1) The natural faces of d-AHT crystals are sphenoidal and prism faces. These faces exhibit features (layers and striations), which represent a mixture of growth and etch patterns. It is difficult to identify them separately.
- (2) The occurrence of striations on prism faces and layers on sphenoidal faces suggests a model, most likely to represent the growth of orthorhombic disphenoidal crystal. The model is



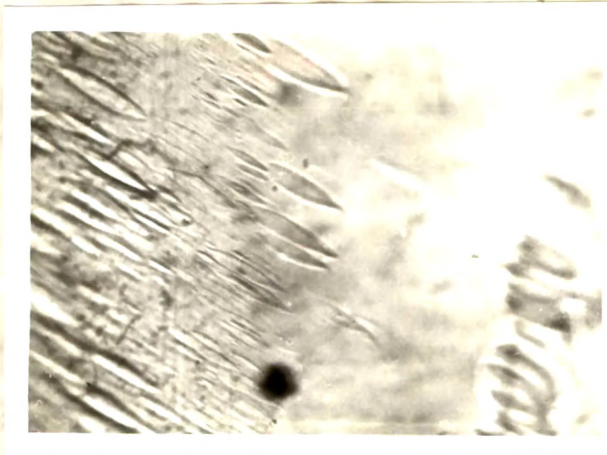
(a)

x200



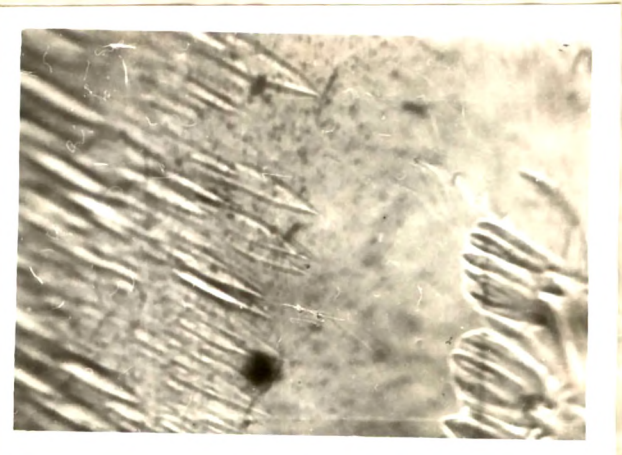
(b)

x200



(c)

x100



(d)

x200

Fig. 8.13 Successive etching of cleavage surface by etchant 15 gm trichloroacetic acid in 100 c.c. glacial acetic acid for 45, 90, 135 and 170 sec. respectively.

formed from a basic unit consisting of a needle with cross-sectional edges parallel to the sphenoidal edges.

- (3) Water, unsaturated solution of d-AHT in water, formic acid and varying amounts of trichloroacetic acid dissolved in fixed quantity of glacial acetic acid preferentially act on a d-AHT surface.
- (4) Etch pits on successive etching of the same cleavage surface and matching of etched cleavage counterparts has shown in a qualitative manner that etch pits are at dislocations ending on the observational plane.
- (5) The average value of density of dislocation etch pits is  $5 \times 10^5 \text{ cm}^{-2}$ .
- (6) The shape cycle of etch pits on a d-AHT cleavage surface is obtainable by progressively increasing the quantity of trichloroacetic acid in a fixed quantity of glacial acetic acid and can be explained on the basis of anisotropic etch rates and eccentricity of etch pits.

## REFERENCES

1. VERMA, A.R. 1951 Phil. Mag. 42, 1005.
2. AUGUSTINE, F. and 1960 J. Phys. Chem. HALE, D.R. Solids 13, 344
3. DESAI, C.C. 1979 Kristall and Technik, 14, 289.
4. JOSHI, M.S., 1980 Kristall and MOHAN RAO, P. and ANTONY, A.V. Technik, 15, 9, 1013
5. FRANK, F.C. 1949 Discussion Faraday Soc. No. 5, 48.
6. GILMAN, J.J. 1958 Dislocation and Mechanical properties of crystals, Wiley, New York.
7. IVES, M. and 1963 Surface Sci. 13, MCAUSLAND, D.D. 189.
8. IVES, M.B. and 1960 J. Chem. Phys., HIRTH, J.P. 33, 817.

9. URUSOVSKAYA, A.A. 1965 Sov. Phys. Cryst.  
10, 437.
10. HARIBABU, V. and 1969 Physica, 30,  
BANSIGIR, K.G. 2003.
11. RAJU BHAGAVAN, 1970 J. Phys. D. 3(12),  
I.V.K. ; 1796.  
SANKARAM BHIMA,  
T. and BANSIGIR,  
K.G.
12. RAJU BHAGVAN, 1971 J. Cryst. Growth,  
I.V.K. and 11(2) 171.  
BANSIGIR, K.G.
13. SANGWAL, K. and 1978 Kristall and  
PATEL, T.C. Technik, 13, 281.
14. POPKOVA, E.G. ; 1970 Kristallografiya,  
PREDVODITELEV, 15(1), 91.  
A.A.
15. POPKOVA, E.G. ; 1969 Kristallografiya,  
MATVEEVA, G.S. 14(1), 53.  
and PREDVODITELEV,  
A.A.
16. PANDYA, N.S. and 1954 Proc. Roy. Soc.  
TOLANSKY, S. A225, 40

17. RAM, U.S. ;  
DUBEY, M. and  
SINGH, G. 1973 International  
Conference on Silicon  
Carbide, Miami Beach,  
Fla. USA 17-20 Sept.
18. TAKOO, R.K. 1985 Cryst. Res. Technol.  
20, 7, 907.
19. BHAGIA, L.J. and  
PANDYA, J.R. 1985 Indian J. Pure and  
App. Phys. 23, 27.
20. SHAH, A.J. and  
PANDYA, J.R. 1985 Crystal Res. &  
Technol. 20, 813
21. MEHTA, B.J. 1972 Ph.D. Thesis, M.S.  
Univ. of Baroda,  
Baroda.
22. ACHARYA, C.T. 1978 Ph.D. Thesis, M.S.  
Univ. of Baroda,  
Baroda.
23. SHAH, R.T. 1976 Ph.D. Thesis, M.S.  
Univ. of Baroda,  
Baroda.
24. BHAGIA, L.J. 1983 Ph.D. Thesis, M.S.  
Univ. of Baroda,  
Baroda.

25. SHAH, A.J. 1984 Ph.D. Thesis, M.S.  
Univ. of Baroda,  
Baroda.
26. MEHTA, B.J. and 1982 Surface Tech. 15,  
PANDYA, J.R. 141.
27. MEHTA, B.J. 1980 Ibid 11, 1301.
28. MEHTA, B.J. 1981 Ibid 12, 253.
29. MEHTA, B.J. 1981 Ibid 13, 73
30. PANDYA, J.R. and 1969 Min. Mag. Lond.  
MEHTA, B.J. 37, 525.
31. PANDYA, J.R. and 1983 Surface Tech. 19,  
BHAGIA, L.J. 187.

## List of Tables

- 8.1 Shape cycle of etch pits produced by varying quantity of crystalline trichloroacetic acid in 100 c.c. of glacial acetic acid at 30°C on a cleavage surface of d-AHT.
- 8.2 Schematic diagram of etch pits produced by formic acid at 30°C, on a cleavage surface of d-AHT.

### Captions to Figures

- Fig. 8.1(A) A Comparative sizes of various crystal habits of d-AHT
- (B) (a,b,c,d,e,f) Photographs of different d-AHT crystal habits with the corresponding line diagrams and faces with their miller indices, where m(110), a(100), d(130) and z(111).
- 8.2 Striations on a prism face (110) parallel to [001].
- 8.3 Layered structure on a sphenoidal face (111) with lines parallel to each other and starting from a sphenoidal edge and ending on the other.
- 8.4 Needle-shaped etch pits of assorted sizes produced by etching d-AHT prism face (110) by distilled water for two seconds.
- 8.4 Model of orthorhombic disphenoidal crystal on the basis of observations on growth and etching.
- 8.5 Trapezoidal etch pit on a cleavage plane (010) produced by formic acid (etching time 5 sec. at 30°C) parallel sides are having direction [001].

- Fig. 8.7a,b Matching of cleavage counter parts etched by formic acid for 5 sec. showing one-to-one correspondence between etch pits.
- 8.8a,b Matching of cleavage counter parts etched by mixture of 5 gm trichloroacetic acid in 100 c.c glacial acetic acid for 60 sec.
- 8.9 Curvilinear trapezoidal etch pits on cleavage plane, by solution of 5 gm trichloroacetic acid in 100 c.c. of glacial acetic acid for 60 sec. at 30°C.
- 8.10 Triangular etch pits on cleavage plane, obtained by etchant 10 gm trichloroacetic acid in 100 c.c. glacial acetic acid for 90 sec. at 30°C.
- 8.11 Elliptical shape etch pits on cleavage surface by 15 gm trichloroacetic acid in 100 c.c. glacial acetic acid for 120 sec. at 30°C.
- 8.12 Leaf-shaped etch pits on cleavage surface by 20 gm trichloroacetic acid in 100 c.c. glacial acetic acid for 180 sec. at 30°C.
- 8.13 Successive etching of cleavage surface by etchant 15 gm trichloroacetic acid in 100 cc glacial acetic acid for 45, 90, 135 and 170 sec., respectively.